Research Paper

DNASE1L3 arrests tumor angiogenesis by impairing the senescence-associated secretory phenotype in response to stress

Deliang Guo[1,*], Dong Ma[1,*], Pengpeng Liu[1,*], Jianwei Lan[1], Zhisu Liu[1], Quanyan Liu[2,&]

[1]Department of Hepatobiliary Surgery, Zhongnan Hospital of Wuhan University, Wuhan 430071, P.R. China
[2]Department of Hepatobiliary Surgery, Tianjin Medical University General Hospital, Tianjin 300052, P.R. China
*Equal contribution

Correspondence to: Quanyan Liu, Zhisu Liu; **email:** lqy@whu.edu.cn; liuzs53@sina.com.cn, https://orcid.org/0000-0003-1156-1236
Keywords: senescence, angiogenesis, hepatocellular carcinoma, DNASE1L3
Received: December 18, 2020 **Accepted:** February 19, 2021 **Published:** March 19, 2021

Copyright: © 2021 Guo et al. This is an open access article distributed under the terms of the Creative Commons Attribution License (CC BY 3.0), which permits unrestricted use, distribution, and reproduction in any medium, provided the original author and source are credited.

ABSTRACT

Hepatocellular carcinoma (HCC) is one of the most challenging and aggressive cancers with limited treatment options because of tumor heterogeneity. Tumor angiogenesis is a hallmark of HCC and is necessary for tumor growth and progression. DNA damage stress and its associated deoxyribonuclease1-like 3 (DNASE1L3) are involved in HCC progression. Here, we explored the influence mechanism of DNASE1L3 on tumor angiogenesis under DNA damage stress in vitro and in vivo. DNASE1L3 was found downregulated and negatively correlated with poor prognosis of resectable and unresectable HCC patients. The tissue microarray of HCC revealed the negative association between DNASE1L3 and cancer vasculature invasion. Mechanistically, DNASE1L3 was found to relieve cytoplasmic DNA accumulation under DNA damage stress in HCC cell lines, in turn cell senescence and senescence-associated secretory phenotype were arrested via the p53 and NF-κB signal pathway, and hence, tumor angiogenesis was impaired. Furthermore, we found that DNASE1L3 excised these functions by translocating to the nucleus and interacting with H2BE under DNA damage stress using co-immunoprecipitation and fluorescence resonance energy transfer assay. In conclusion, DNASE1L3 inhibits tumor angiogenesis via impairing the senescence-associated secretory phenotype in response to DNA damage stress.

INTRODUCTION

Hepatocellular carcinoma (HCC) is one of the most common digestive malignancies worldwide. Although treatments such as radical surgery, chemotherapy, radiotherapy and target therapy are of value in the management of these tumors, the prognosis of patients diagnosed with HCC remains grave. Thus, it is still a major risk factor threatening human health [1–5]. Multiple factors have been confirmed in the etiology of HCC, including hepatitis B or C virus (HBV or HCV) infections, obesity, alcohol consumption and dietary pollution [6]. These factors are also associated with chronic liver damage and inflammation, which can promote DNA damage and chromosome aberrations, as well as trigger a series of signaling pathways. One major downstream signaling route is via the DNA damage response (DDR) pathway, which is involved in DNA repair regulation and cell cycle arrest, eventually leading to cell death or senescence [7]. Meanwhile, DDR aberrations can destroy genomic integrity, trigger liver cancer pathogenesis, and promote the development of advanced HCC [8]. Therefore, a better understanding of the DDR pathway would help in developing strategies to treat or prevent HCC.

One of the outcomes of activating the DDR is the induction of cellular senescence [7]. Senescence is a process that limits the proliferation of damaged or aging cells in response to multiple types of stress, including

DNA damage, telomere shortening and oncogene activation. It is involved in different biological processes, such as carcinogenesis, aging, wound healing, tissue repair and embryogenesis [9]. DNA double-strand breaks, loss of the nuclear lamina protein Lamin B followed by internal and external stresses [10] leads to the appearance of chromatin fragments in the cytoplasm, which eventually activates the cytosolic DNA sensing machine to affect cellular senescence phenotype [11]. During the oncogenesis and development of HCC, cellular senescence acts as a double-edged sword [12]. It prevents the proliferation of damaged cells, thereby preventing tumors from occurring, and also affects the tumor microenvironment by secreting chemokines, proteases and pro-inflammatory cytokines, which are called SASP [8]. DDR defects give rise to genomic instabilities that enhance cancer occurrence and progression through mutation accumulation, unbalancing cellular senescence and apoptosis by inhibiting the cytoplasmic DNA sensing signal pathway. In addition, these defects exhibit targetable vulnerabilities that are relatively specific to cancer cells. For example, DDR inhibitors or regulators can benefit clinical outcome of multiple cancers [13].

DNASE1L3 is a secreted DNase homologous to DNASE1, it is capable of both single- and double-stranded DNA cleavage [14]. It has a unique capacity for digesting membrane-encapsulated DNA, and has a preferential capacity to digest DNA within nucleosomes during apoptosis and necrosis [15]. In combination with DNASE1, it plays a key role in the degradation of neutrophil extracellular traps and cfDNA which in turn reduce organ damage following inflammation [16]. However, differing from its other homologs (DNASE1, DNASE1L1, DNASE1L2), DNASE1L3 contains two functional nuclear localization signals (NLSs) in the mature protein that allows it to shuttle into the nucleus [17]. Thus, whether DNASE1L3 participates in the accumulation of cytoplasmic DNA which in turn affects the progression of HCC via regulating the tumor microenvironments was elucidated.

In this study, we found that downregulated DNASE1L3 expression correlates with poor prognosis of HCC patients. Up-regulated expression of DNASE1L3 relieves cytoplasmic DNA accumulation under DDR activation, in turn cell senescence and SASP were arrested, tumor angiogenesis was impaired. We also found that DNASE1L3 excises these functions through interacting with H2BE. These results indicate DNASE1L3 is a potential biomarker for predicting the prognosis of HCC and identify DNASE1L3 as a regulator of tumor microenvironment via impairing the senescence-associated secretory phenotype in response to stress.

RESULTS

DNASE1L3 is downregulated in human HCC tissues and positively correlated with prognosis in resectable HCC

To assess the clinical significance of DNASE1L3 for HCC patients, we first analyzed several publicly available RNA datasets of HCC from The Cancer Genome Atlas (TCGA) and Oncomine database (https://www.oncomine.org). The mRNA expression levels of DNASE1L3 in multiple types of tumors were lower compared with non-tumor tissues. In addition, the expression differences are also significant in multiple HCC cohorts (Supplementary Figure 1A, 1D). Kaplan-Meier curves for the overall survival (OS) and disease-free survival of HCC patients from the TCGA database showed patients with higher mRNA expression level of DNASE1L3 exhibited better prognosis than those with lower expression profile (Supplementary Figure 1B).

To further determine the expression pattern of DNASE1L3 in HCC, we examined the mRNA expression level of DNASE1L3 in 125 paired HCC samples and adjacent non-tumor tissue samples by quantitative real-time PCR (RT-qPCR). The results showed that DNASE1L3 was downregulated in HCC tissues (Figure 1A). To assess the protein expression level of DNASE1L3 in HCC, immunohistochemistry (IHC) analysis was performed using HCC tissue microarray containing 204 paired tumor and para-tumor tissues. The histological scores of DNASE1L3 in paired tissues were evaluated. The results showed the protein expression level was downregulated in HCC tissues (Figure 1B, 1C), consistent with the RT-qPCR results. We then confirmed these findings using Western blotting in another cohort of 21 paired fresh HCC tissues (Figure 1D). These results indicated that the DNASE1L3 protein expression was lower in HCC tissues.

To evaluate the relationship between DNASE1L3 protein expression and clinical pathological features, the cohort of 204 HCC patients subjected to IHC histological scoring was analyzed. Importantly, the results showed that downregulated DNASE1L3 protein expression was significantly associated with advanced tumor size, number of tumors and microvascular invasion (Supplementary Table 1). Kaplan-Meier analyses showed a significant association between low DNASE1L3 expression and poor prognosis of HCC (Figure 1E, 1F). Furthermore, multivariate logistic regression analyses indicated that DNASE1L3 acts as an independent prognostic factor of HCC (Figure 1G and Supplementary Table 2).

DNASE1L3 was downregulated in the plasmas of HCC patients and was positively correlated with prognosis in unresectable HCC

Since DNASE1L3 is also an extracellular secreted protein [18], furthermore, we analyzed plasma DNASE1L3 protein levels in another cohort of 95 cases encompassing 50 inoperable HCC patients, 27 patients with hepatitis only and 18 healthy individuals. HCC patients exhibited a significantly lower DNASE1L3 levels compared to the normal group, but higher than patients with hepatitis only (Figure 1H). The 50 inoperable HCC patients undergone

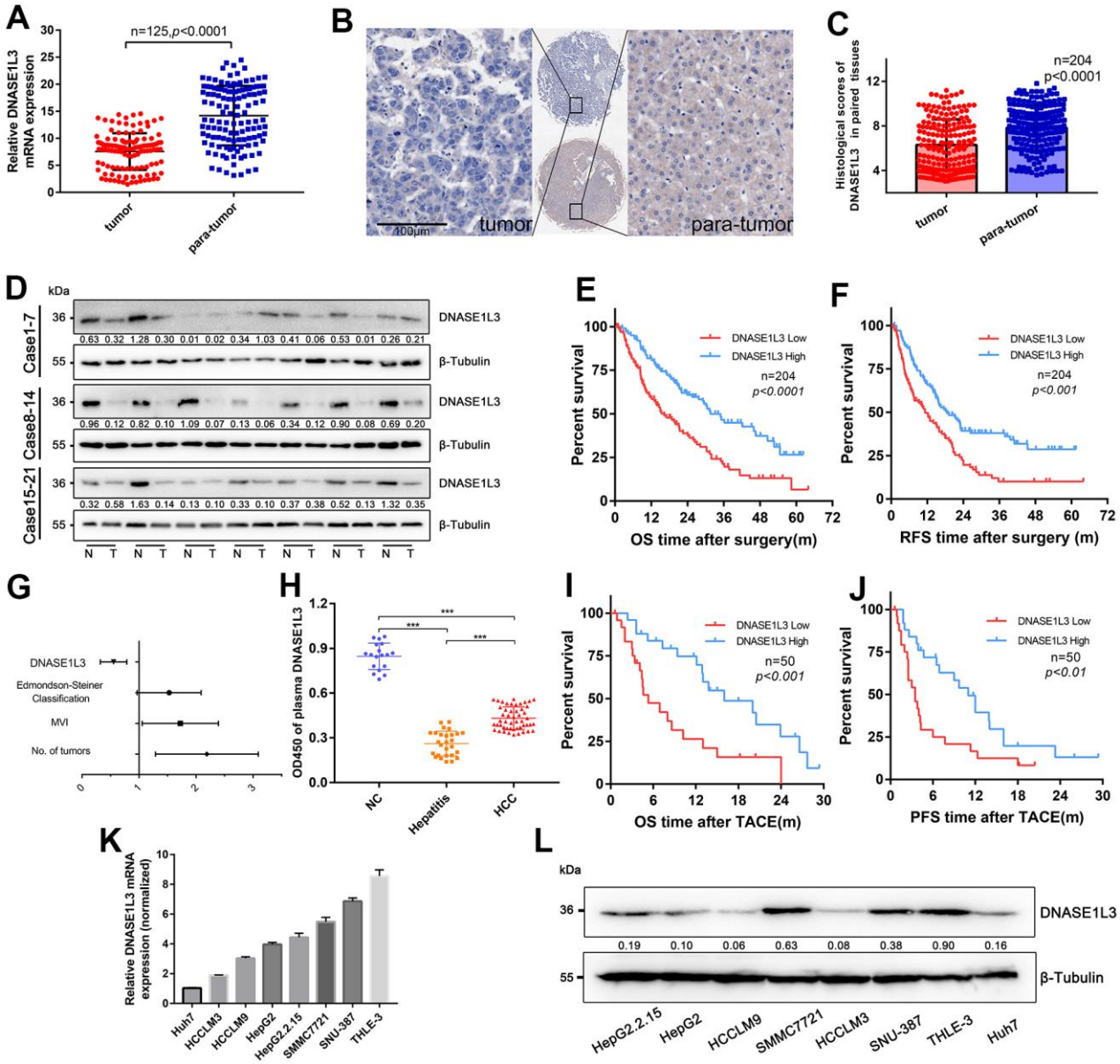

Figure 1. Downregulated DNASE1L3 is positively correlated with prognosis of resectable or unresectable HCC. (**A**) The transcriptional level of DNASE1L3 was down-regulated in HCC tissues(n=125) compared to paired para-tumor tissues as tested by RT-qPCR. (**B**) Representative images of IHC staining for DNASE1L3 in HCC and adjacent normal tissues (scale bar, 50 μm). (**C**) The histological scores of DNASE1L3 in 204 paired tissues of HCC was evaluated. (**D**) The translational level of DNASE1L3 between HCC tissues and paired adjacent non-tumor tissues from 21 patients were identified by western blotting. ("T" for tumor, "N" for non-tumor). (**E**, **F**) Kaplan-Meier survival curves of OS and RFS time for 204 patients with HCC. (**G**) Forest plot of risk factors of the OS time using multivariate Cox regression analysis. (**H**) Comparison of plasma levels of DNASE1L3 between patients of HCC(n=50), patients of hepatitis only(n=27) and healthy individuals(n=18). (**I**, **J**) Kaplan-Meier survival curves of OS and PFS time for 50 patients with inoperable HCC. (**K**) RT-qPCR analysis of DNASE1L3 in HCC cell lines and a normal liver cell line (THLE-3). (**L**) Western blot analysis of DNASE1L3 protein expression in HCC cell lines and a normal liver cell line (THLE-3).

repeated transcatheter arterial chemoembolization treatment (TACE) and other followed treatments. Kaplan-Meier analyses showed a significant association between low DNASE1L3 expression and poor prognosis in patients with inoperable HCC after TACE (Figure 1I, 1J). We also evaluated the OS and progression-free survival (PFS) time in a cohort of patients treated with sorafenib [19] using KM plotter. The results revealed that low expression levels of DNASE1L3 were associated with lower insensitivity of sorafenib treatment (Supplementary Figure 1C).

Finally, we explored the transcriptional and translational levels of DNASE1L3 in the immortalized normal human hepatic cell line THLE-3 and multiple HCC cell lines, including the SMMC7721, SNU-387, HepG2, HepG2.2.15, HCCLM3 HCCLM9, and Huh7 cell lines. The transcriptional and translational levels of DNASE1L3 found to be suppressed in most HCC cell lines compared to the THLE-3 cell line (Figure 1K, 1L). Taken together, these data implied that the DNASE1L3 protein level is lower in HCC and is closely correlated with poor prognosis of HCC.

Overexpression of DNASE1L3 relieves cytoplasmic DNA accumulation under DDR activation

Since DDR activation induces cytoplasmic DNA accumulation while the DNase enzymes function as digester of DNA [20], we evaluated the hypothesis that DNASE1L3 may relieve cytoplasmic DNA accumulation under DDR activation. Upon establishing stable DNASE1L3-overexpressing hepatoma cells, DDR was separately induced by UV and H_2O_2. Cytoplasmic accumulation of nuclear DNA and DDR were assessed by DNA damage foci (DDF) number (Figure 2A, 2B), reduced DNA synthesis (Supplementary Figure 2A), and qPCR analysis of chromosomal DNA in the cytoplasmic fraction (Figure 2C, 2D). Overexpression of DNASE1L3 inhibited cytoplasmic DNA accumulation

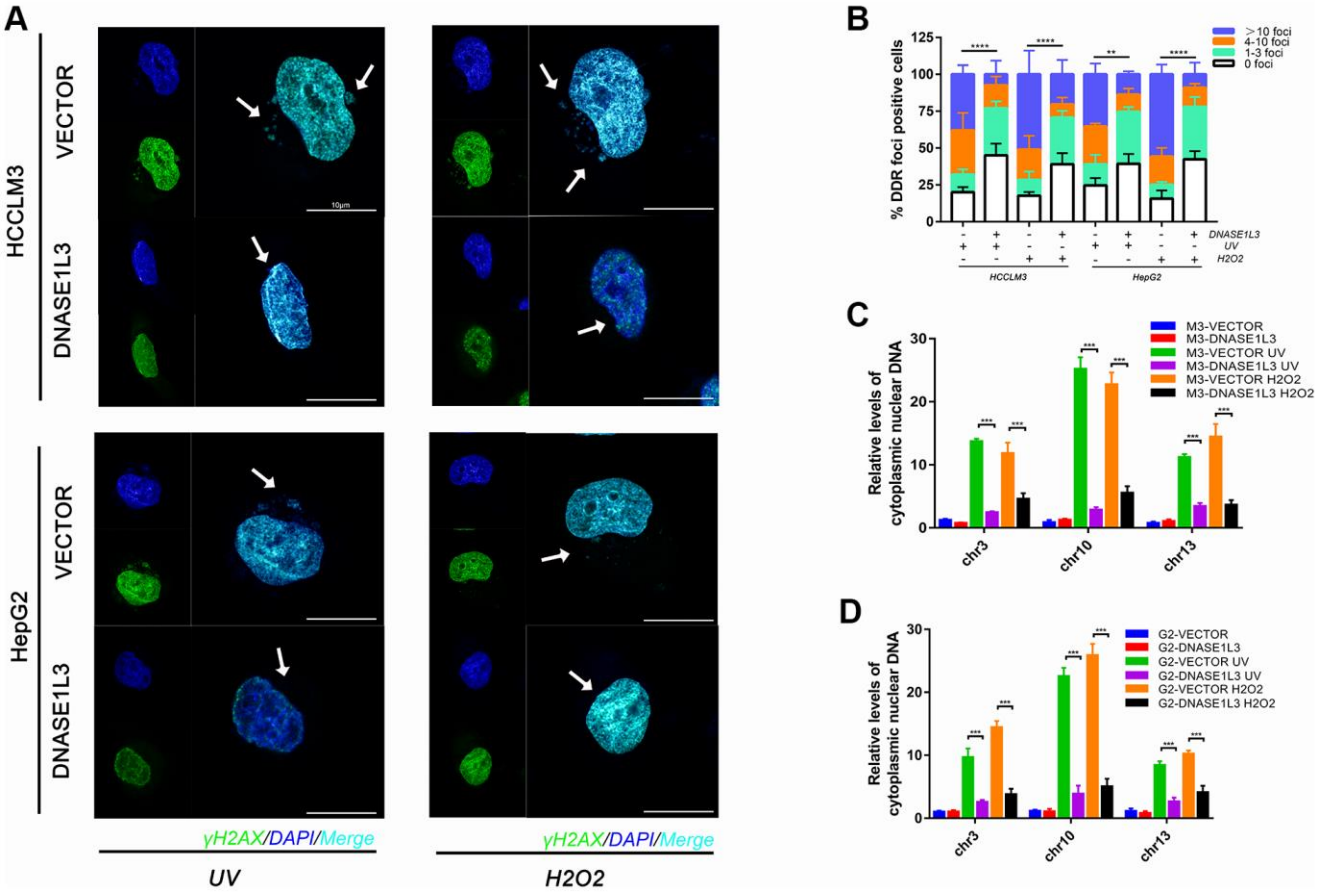

Figure 2. Overexpression of DNASE1L3 relieves cytoplasmic DNA accumulation under DDR activation. (**A**) Cytoplasmic accumulation of nuclear DNA in differentially treated cells were assessed, representative images were shown (green, γH2AX; blue, DAPI; Scale bars, 10 μm). (**B**) Quantification of DNA damage foci (DDF). The number of DDF per cell falls into each of the 0, 1-3, 4-10, and >10 counting categories. At least 100 cells counted per group. (**C**, **D**) qPCR analysis of chromosomal DNA in cytoplasmic fraction of cells treated in different group.

while knockdown DNASE1L3 exacerbate the phenotype under DDR activation (Supplementary Figure 3A–3D), at least in certain cultured cell types and such inducing conditions.

Overexpression of DNASE1L3 relieves cell senescence and SASP under DDR activation

The prominent concordance between distinctive DNASE1L3 expression and cytoplasmic DNA accumulation under DNA damage response observed in HCC cancer cells prompted us to further explore the functional implications of DNASE1L3 in damaged cells. Notably, UV or H_2O_2 treatment induced evident cellular senescence, as indicated by positive SA-β-Gal staining and remarkable morphological alterations. Interestingly, after the induction of DNA damage, both cell lines changed their morphology to resemble a stellate or fusiform morphology with projections, sometimes numerous (Figure 3A). Under DDR activation, DNASE1L3 overexpressed cell lines relieved cell senescence when compared to the vector groups (Figure 3A, 3B). Meanwhile, knockdown of DNASE1L3 made more cells senesced (Supplementary Figure 3F, 3G). However, DNASE1L3 was not shown to affect the senescence ratio without UV or H_2O_2 treatment.

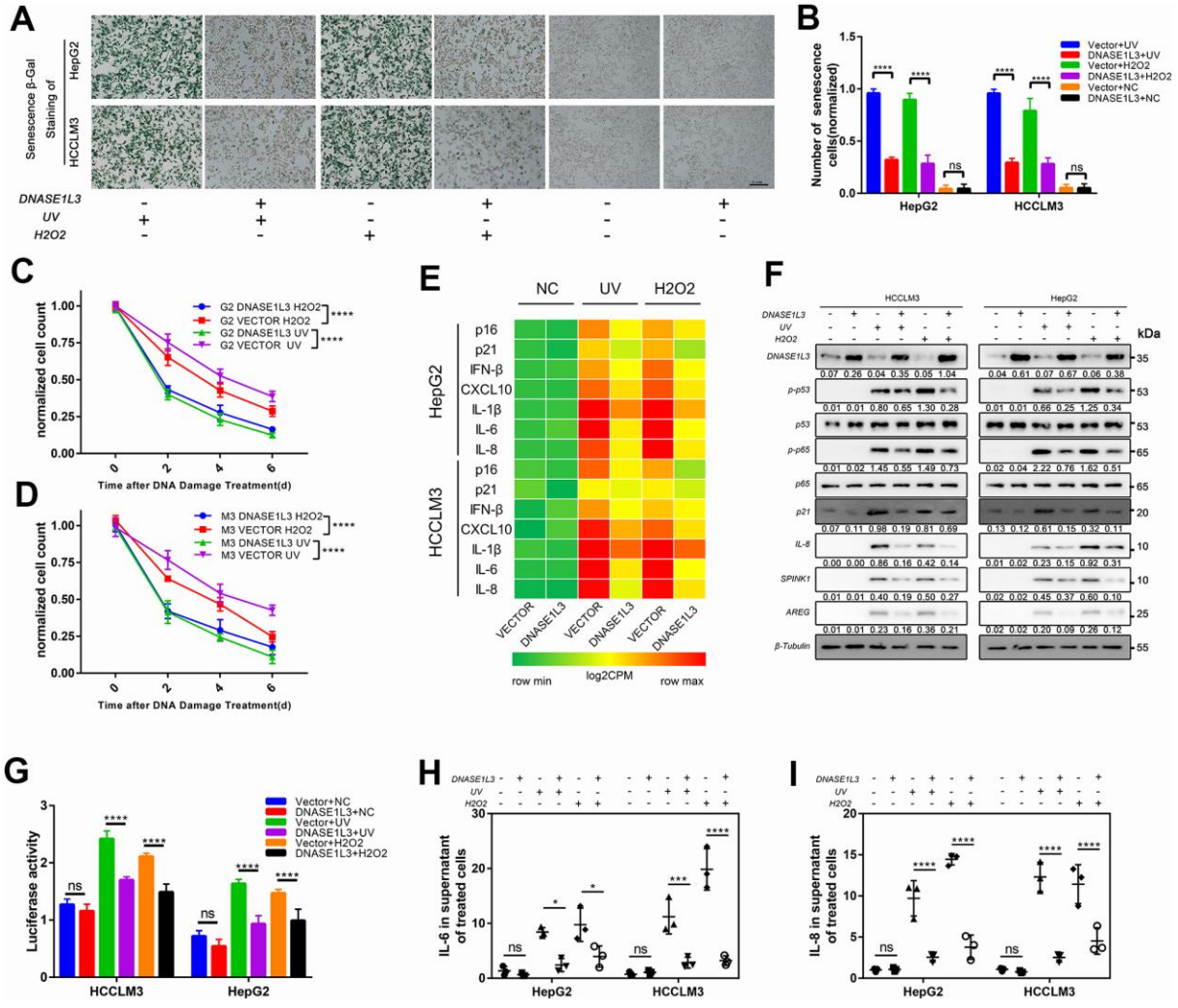

Figure 3. Overexpression of DNASE1L3 relieves cell senescence and SASP under DDR activation. (**A**) Representative images of SA-β-Gal staining of cells in differently treated groups (scale bar, 200 μm). (**B**) Statistics of SA-β-Gal staining cells in differently treated groups. (**C**, **D**) Remnant cell number were analyzed by cell counts enumerated from differently treated groups at various time points. (**E**) Transcriptional level of canonical SASP factors in differently treated groups, with values normalized to the vector control per factor. The heatmap for the mean RT-qPCR data is shown. (**F**) Immunoblot analysis of inducible expression change of senescence associated signal pathway and downstream proteins including p53, p65, SPINK1 and AREG in different treated groups. (**G**) Dual luciferase assay showed activated NF-kB signaling in different treated groups. (**H**, **I**) ELISA analysis of IL-6, IL-8 secretion in supernatants from cells in different treated groups.

Depending on the level of DNA damage, accumulated DNA damage induces cellular apoptosis or senescence [21, 22]. Therefore, we determined whether over-expression of DNASE1L3 could initiate the apoptosis of DNA damaged cells. It was found that the overexpression of DNASE1L3 enhances cell apoptosis in the early stage (day 1to3) after DNA damage (Supplementary Figure 2B). In the late stage (day 7to10) post DNA damage, the remaining cell in the cultures were counted and illustrated in Figure 3C, 3D. The results showed less cells remaining in the culture in DNASE1L3 overexpressed group compared with vector group after DNA damage treatments. Interestingly, even without DNA damage treatments, DNASE1L3 could mildly promotes the apoptosis of HCC cell lines (data not shown here).

Accompanied with the decreased cellular senescence, the expression of IFN-β, a downstream mediator of the cytoplasmic DNA sensing machinery [20], and the other canonical SASP factors such as IL-6, IL-8, CXCL10, SPINK1 and AREG [20, 23] were examined by RT-qPCR, western-blotting or elisa assays (Figure 3E, 3F, 3H, 3I and Supplementary Figure 3E). As supporting evidence, whether the p53-p21 cell arrest signal pathway and NF-κB signal pathway could be impaired by DNASE1L3 was checked by western-blotting and dual luciferase reporter assay. The results obtained from cells in the late stage post DNA damage showed DNASE1L3 suppresses the activation of p53-p21 signal pathway and NF-κB signal pathway under DDR activation (Figure 3F, 3G and Supplementary Figure 3E).

DNASE1L3 impairs angiogenesis through differential expression of SASP under DDR activation

The expression of DNASE1L3 is associated with the prognosis of HCC with DNA damage treatment or anti-angiogenesis such as TACE or solafenib (Figure 1 and Supplementary Figure 1). Meanwhile, it affects cell senescence and SASP which contain plenty of chemokines, cytokines, and growth factors by cytoplasmic DNA accumulation. We hypothesized that DNASE1L3 affects angiogenesis when DDR is activated. To test this hypothesis, a tissue microarray with 40 HCC samples was used, and the association between DNASE1L3 and CD34 Chalkley count was assessed. Low expression of DNASE1L3 was considerably associated with cancer vasculature invasion (Figure 4A). Tumor tissues of DNASE1L3 intermediately or highly expressed were observed to be linked with lower vasculature invasion (Figure 4B, 4C). The result showed the histological scores of DNASE1L3 was negatively associated with the CD34 Chalkley counts in HCC tissues (Figure 4D). To further confirm the results obtained from the tissue model, we examined HUVEC motility, migration and tube formation using supernatants from cancer cell lines with or without DDR treatments. The results showed, without DDR treatment, the supernatants collected from cell lines overexpressing DNASE1L3 could not initiate the motility, migration and tube formation capacity of HUVEC cells (Figure 4E–4J). However, when DDR was activated with UV or H_2O_2 treatments in cancer cells, the angiogenesis of HUVEC cells was enhanced by the supernatants of the treated cells. The opposite phenomenon was observed when knockdown of DNASE1L3 (Supplementary Figure 3H–3K). Accordingly, DNASE1L3 could relives the motility, migration and tube formation ability of HUVEC cells by regulating differential SASP expression of cancer cell lines under DDR activation, at least in certain cultured cell types and such inducing conditions.

DNASE1L3 interacts with H2BE

DNASE1L3 was reported possessed two nuclear localization signal peptides [24]. Meanwhile, VP-16, a topoisomerase inhibitor interferes with the action of topoisomerase enzymes (topoisomerase I and II), in turn causes single-strand and double-strand breaks in DNA and produces cytotoxicity, could facilitate DNASE1L3 translocation to the nucleus [25]. We identified DNASE1L3 relieved the cytoplasmic DNA accumulation under DDR activation (Figure 2). Thus, we assume that DNASE1L3 may digest the damaged DNA fractions via enhancing translocation to the nucleus. In order to further validate this conclusion, we performed the nucleocytoplasmic separation followed by western blot experiments, using cell lines with or without UV or H_2O_2 treatments. The results showed the translocation to the nucleus of DNASE1L3 was enhanced upon DDR activation (Figure 5A–5C).

At this point, the mechanism of how DNASE1L3 finish the digest of damaged DNA fractions puzzled us. We analyzed IntAct Molecular Interaction Database (https://www.ebi.ac.uk/intact/interaction/EBI-20919708) and checked coIP-MS results in our previous experiment(unpublished). The DSSO crosslink assay showed DNASE1L3 could bind to H2BE [26], previous coIP-MS results (Supplementary Figure 4A) showed DNASE1L3 have connections with multiple histones (H3, H2AJ, H2A1C, etc.). All these findings indicate that DNASE1L3 may exert its functions by binding H2BE. To validate the physical interactions between DNASE1L3 and H2BE, we enforced the expression of Flag-H2BE and cMyc-DNASE1L3 in 293T cells for reciprocal immunoprecipitation and confirmed associations between the two proteins (Figure 5D). Moreover, co-immunoprecipitation using HepG2 and HCCLM3 cell lysates validated the specific interaction between endogenous DNASE1L3 and H2BE in HCC

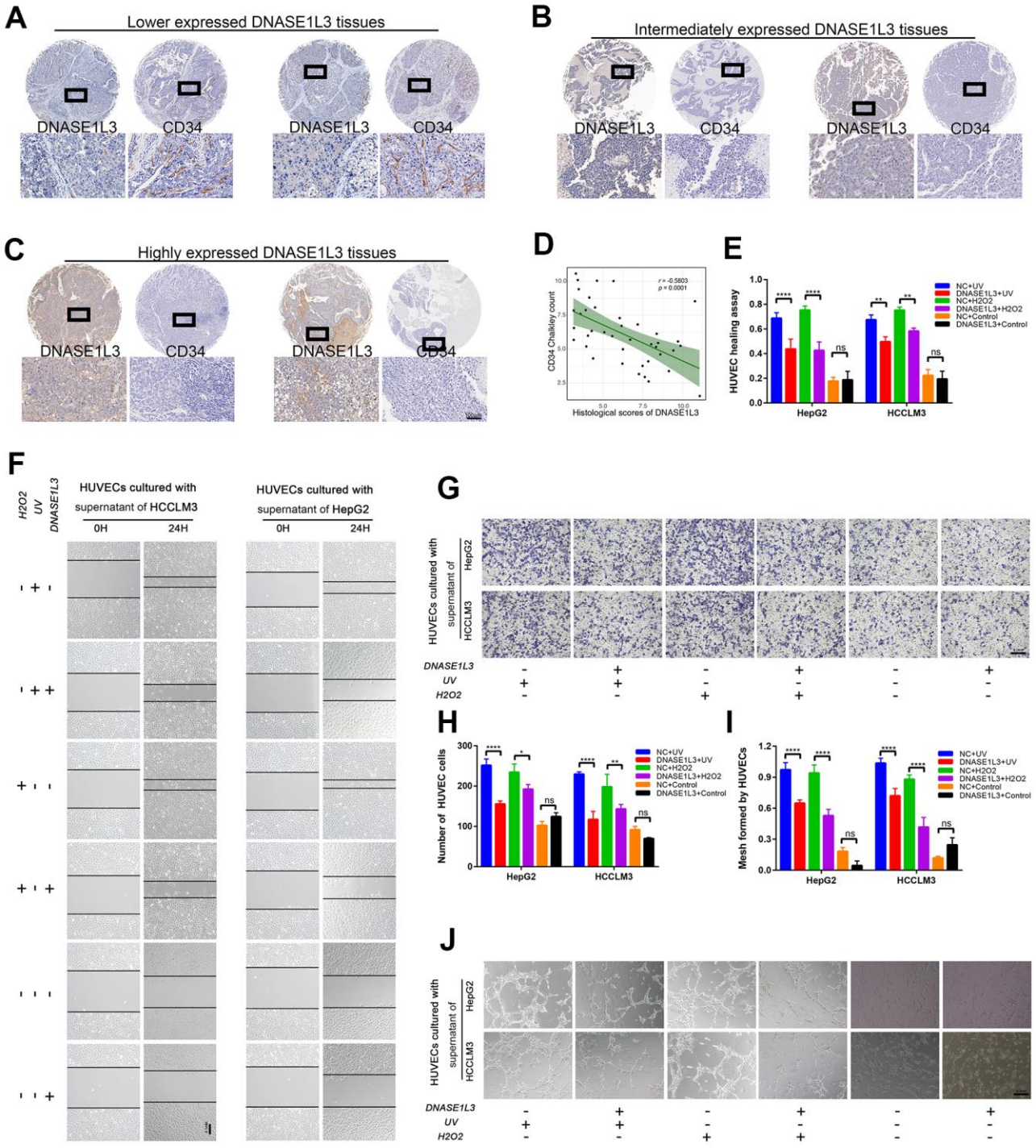

Figure 4. DNASE1L3 impairs angiogenesis through the differential expression of SASP under DDR activation. (**A**) Tissue microarray was stained with anti-DNASE1L3 and anti-CD34 antibody, low expression of DNASE1L3 was considerably associated with cancer vasculature invasion. (scale bar, 100 μm). (**B**, **C**) Tumor tissues of DNASE1L3 intermediately or highly expressed were observed to be linked with lower vasculature invasion. (scale bar, 100 μm). (**D**) The histological scores of DNASE1L3 and the CD34 Chalkley counts in HCC tissues was analyzed and showed a significant negative association. (**E**, **F**) The motility of HUVECs were assessed by wound healing assay, the supernatants from cells in differently treated groups were added into the culture of HUVECs, images were taken at 0h and 24h (scale bar, 100 μm). (**G**, **H**) The cellular migration ability of HUVECs were determined by the transwell migration assay. The supernatants from cells in differently treated groups were added into the lower chamber, images were taken after 24h of incubation (scale bar, 100 μm). (**I**, **J**) The tube formation ability of HUVECs were determined by tube formation assay. The supernatants from cells in differently treated groups were added into the culture, images were taken after 6h of incubation (scale bar, 100 μm). The results show the means ± SD from at least three separate experiments.

cells (Figure 5E). To substantiate this binding preference, we then used a fluorescence resonance energy transfer (FRET) assay to assess the relative proximity of DNASE1L3 and H2BE in live cells. In HepG2 cells, co-expression of YFP-DNASE1L3 and H2BE-CFP produced FRET, which demonstrated an association between DNASE1L3 and H2BE (Figure 5F).

To define the precise region of H2BE DNASE1L3 binding with for this interaction, we enforced the full-length cMyc-tagged DNASE1L3 in combination with Flag-tagged respective fragments of H2BE in HepG2 cells (Figure 5G). The N-terminal region of H2BE (amino acids 1-28) is the area on the protein surface, and it is not winded by DNA sequence (Supplementary Figure 4B). We deleted this domain and reconstructed a H2BEΔ (Supplementary Figure 4C). Interestingly, the truncated protein lost the ability to interact with DNASE1L3 (Figure 5G), suggesting that the interacting module likely resides in amino acids 1-28.

DNASE1L3 impairs angiogenesis by interacting with H2BE

All of our analyses described thus far suggest that the N-terminal region of H2BE may contribute to the function of DNASE1L3 excised in SASP associated angiogenesis under DDR activation. To test this idea, we next sought to determine the rescue experiments using the truncated protein, Flag-tagged H2BEΔ. Interestingly, we noted that the cytoplasmic DNA accumulation increased when co-transfect H2BEΔ with DNASE1L3 compared with vector and DNASE1L3 (Figure 6A). Cell senescence was also enhanced in the following SA-β-Gal staining assay (Figure 6B, 6C). We also assessed p53-p21 and NF-κB signaling pathways under DDR activation, without the N-terminal region of H2BE, the function of DNASE1L3 was restricted (Figure 6D). We continued to validate its impact on angiogenesis under DDR activation. HUVEC motility, migration and tube formation assays using supernatants

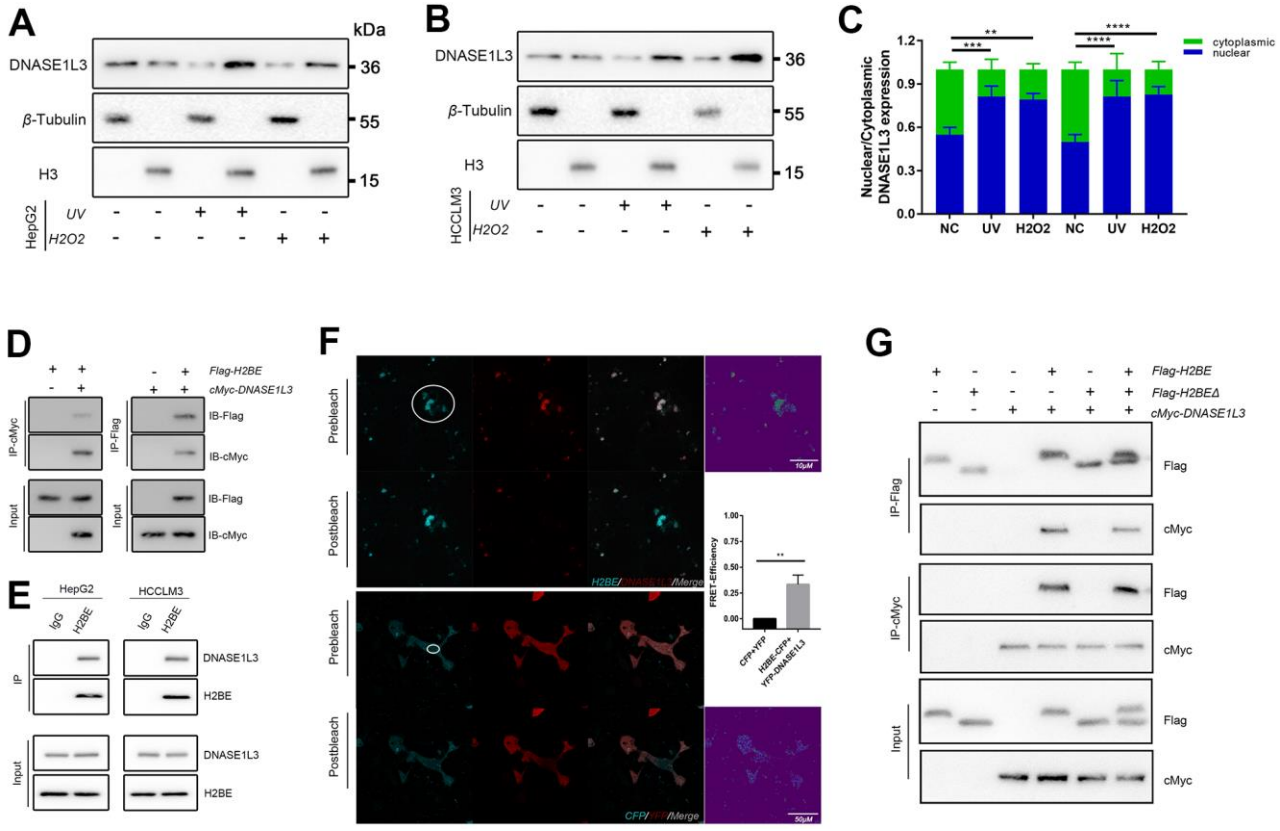

Figure 5. DNASE1L3 interacts with H2BE. (**A**, **B**) Immunoblot analysis of DNASE1L3 in the subcellular localization under DNA damage using nucleocytoplasmic separation in two cell lines. (**C**) The result of blotting confirmed that DNASE1L3 translocated to the nucleus in response to DDR activation. (**D**) Lysates of 293T cells overexpressing Flag-H2BE and/or cMyc-DNASE1L3 were subjected to reciprocal co-immunoprecipitation (co-IP) to detect protein interaction. (**E**) HepG2 and HCCLM3 cell lysates were subjected to co-IP and immunoblot to detect endogenous H2BE and DNASE1L3 interaction. (**F**) FRET assay for DNASE1L3-H2BE interactions in living cells. FRET efficiency were calculated by Leica TCS SP8 software ($FRET_{eff}$= (D_{post}-D_{pre})/D_{post}). White circles identify FRET area. (**G**) Co-IP of cMyc-DNASE1L3 and Flag-tagged H2BE or H2BEΔ with N-terminal region (amino acids 1-28) deleted.

from H2BEΔ co-transfected HepG2 cells with or without DDR treatments were performed (Figure 6E–6J). The results strongly suggest the involvement of both the N-terminal region of H2BE and DNASE1L3 in tumor angiogenesis through regulating senescence-associated secretory phenotype in response to stress.

DNASE1L3 arrests tumor angiogenesis via regulating senescence-associated secretory phenotype in response to stress

The matrigel plug assay was used to assess the ability of DNASE1L3 to inhibit angiogenesis *in vivo*. Matrigel plugs supplemented with supernatants of genetically edited cells with or without DNA damage treatments were subcutaneously injected into mice (Figure 7A). The plugs were then excised, photographed, and assessed for hemoglobin content and CD34 positive area 10 days after injection. Angiogenesis levels within the plugs were evaluated by the degree of hemoglobin content. The plugs were sliced and CD34 positive areas were evaluated. The matrigel supplemented with the supernatant of DNASE1L3 overexpressed cells treated by UV or H_2O_2 exhibited a lighter color depth compared to the vector group, but deeper than cells without DNA damage treatment (Figure 7B). The

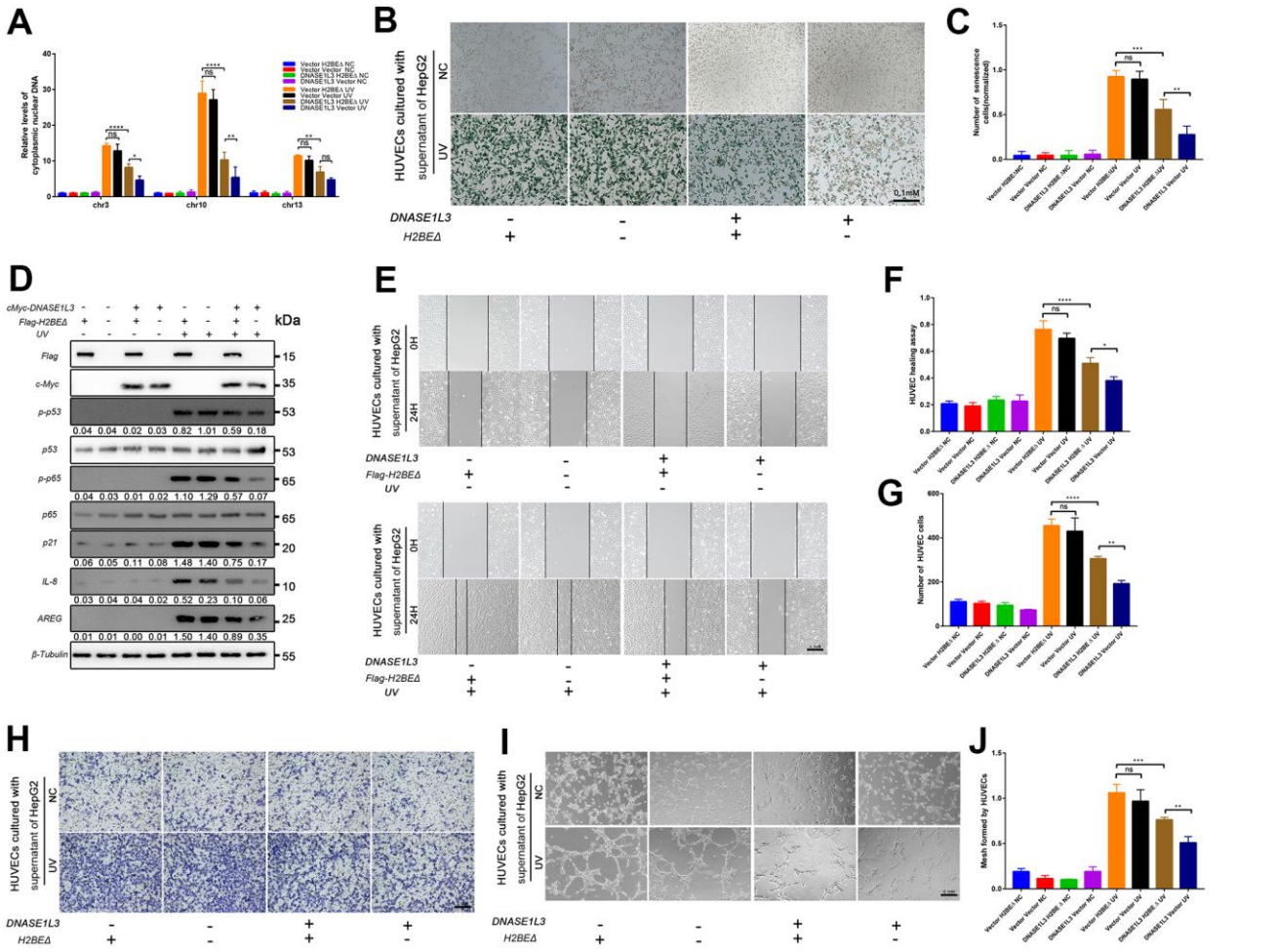

Figure 6. DNASE1L3 impairs angiogenesis by interacting with H2BE. (**A**) qPCR analysis of chromosomal DNA in the cytoplasmic fraction of differently treated HepG2 cells. (**B**) Representative images of SA-β-Gal staining of cells in differently treated groups (scale bar, 100 μm). (**C**) Statistics of SA-β-Gal staining cells in differently treated groups. (**D**) Immunoblot analysis of inducible expression change of senescence associated signal pathway and downstream proteins including p53, p65, SPINK1 and AREG in differently treated groups. (**E**, **F**) The motility of HUVECs were assessed by wound healing assay, the supernatants from cells in different treated groups were added into the culture of HUVECs, images were taken at 0h and 24h (scale bar, 100 μm). (**G**, **H**) The cellular migration ability of HUVECs were determined by the transwell migration assay. Cell supernatants from in differently treated groups were added into the lower chamber, images were taken after 24h of incubation (scale bar, 100 μm). (**I**, **J**) The tube formation ability of HUVECs were determined by tube formation assay. Cell supernatants from differently treated groups were added into the culture, images were taken after 6h of incubation (scale bar, 100 μm). The results show the means ± SD from at least three separate experiments.

observed difference in the tint was confirmed by quantification of hemoglobin and CD34 positive areas (Figure 7C, 7D).

Finally, we further established a subcutaneous tumor model to investigate the role of DNASE1L3 in tumor angiogenesis. Mice were inoculated with Hepa1-6 cells first, then supernatants of different groups of cells treated by UV or H_2O_2 treatments were injected through the tail vein, twice per week, for 2 weeks for a total of four doses (Figure 7E). Vascular density was quantified by CD34 Chalkley count under IHC. The results show

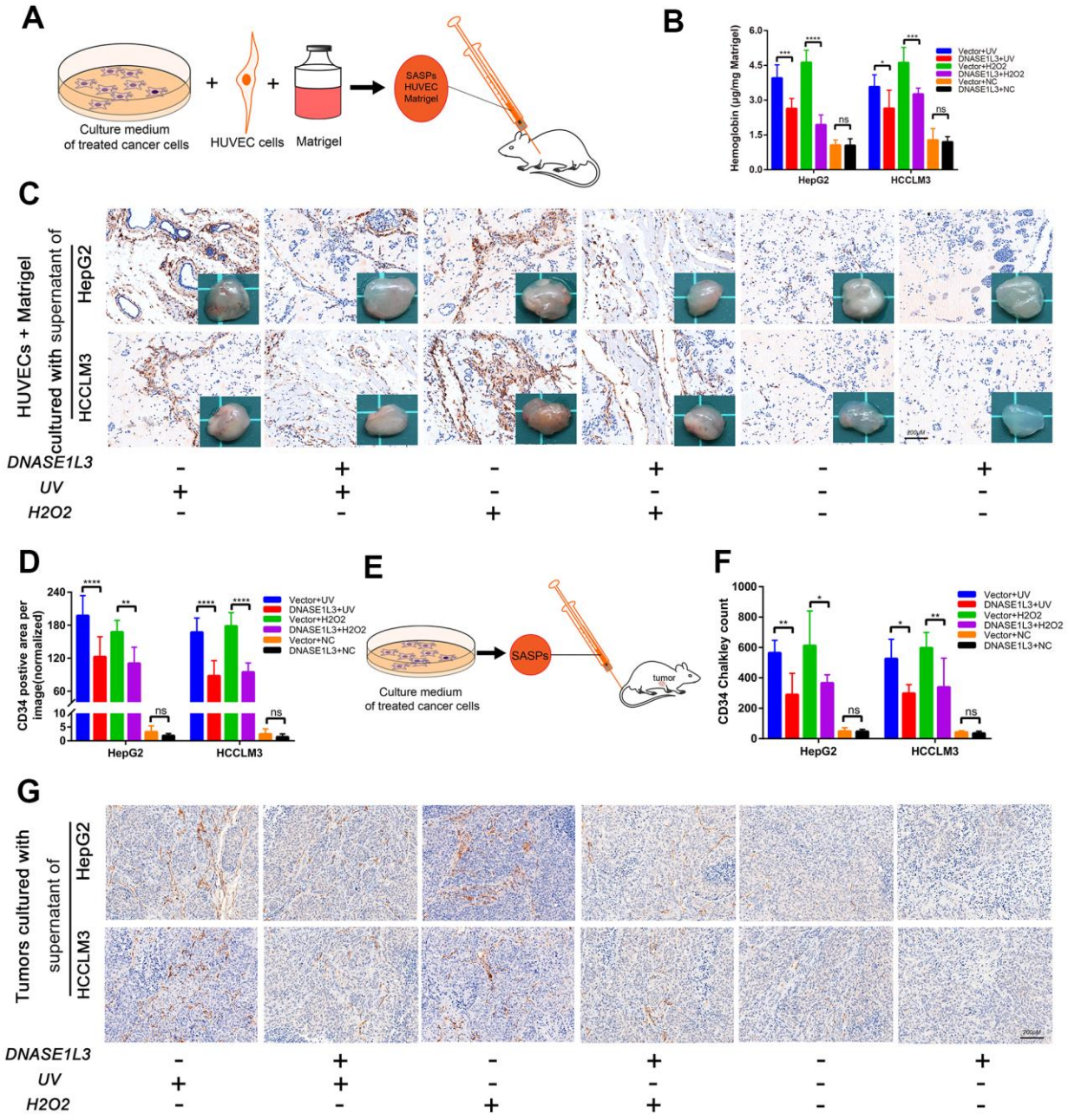

Figure 7. DNASE1L3 arrests tumor angiogenesis by regulating the senescence-associated secretory phenotype in response to stress. (**A**) Matrigel plugs supplemented with cell supernatants from differently treated groups were subcutaneously injected into mice. (**B**) Hemoglobin content was assessed at day 10 after injection. (**C**) Representative images of CD34 staining of the matrigel plugs in differently treated groups (scale bar, 200 μm). Gross view observation of the matrigel plugs were shown in the bottom right corner of each figure. (**D**) CD34 positive area was evaluated in each group. (**E**) Constructed subcutaneous tumor model was used to investigate the role of DNASE1L3 in tumor angiogenesis. (**F**) Vascular density was quantified by CD34 Chalkley count under IHC. (**G**) Representative images of CD34 staining of subcutaneous tumors in differently treated groups (scale bar, 200 μm).

DNASE1L3 arrests tumor angiogenesis through the secretions from cells treated with DDR activation (Figure 7F, 7G). These *in vivo* results, coupled with the *in vitro* and *ex vivo* observations, strongly suggest that DNASE1L3 is a suppressor of angiogenesis.

DISCUSSION

Our findings from the present study fill some gaps between the poor prognosis of HCC and the low expression of DNASE1L3. Our data indicates that DNASE1L3 excises the function in dealing with the accumulated cytoplasmic DNA of nuclear origin provoked by DNA damage. This event results in the relief of DNA damage response, in turn down regulates the occurrence of cellular senescence which affects the tumor angiogenesis through senescence-associated secretions into the microenvironment (see model in Figure 8).

DNASE1L3 is distributed in the endoplasmic reticulum, cytosol, nucleus and extracellular space [16, 27]. It translocates to the nucleus upon cleavage of its endoplasmic reticulum-targeting motif during apoptosis [28, 29]. In our experiments, DNASE1L3 translocates from the cytoplasm to the nucleus in response to UV or H_2O_2 induced DNA damage. As an intracellular endonuclease, it has been investigated that DNASE1L3 associates with DFFB to digest DNA and fragment it into internucleosomal repeats of 153-200 bp [18, 30–32]. The DFFB is involved in the initial cleavage of DNA into 50kb fragments, but not sufficient for acetaminophen-induced internucleosomal DNA fragmentation [32]. Cells deficient in DFF45 lack the ability to generate such DNA fragments in response to various inducers of apoptosis, but have the capacity of resist apoptotic inducers [25]. DNASE1L3 mediates acetaminophen-induced internucleosomal DNA fragmentation [33]. In this study, overexpression of DNASE1L3 enhanced the apoptosis of DNA damaged HCC cell lines. This indicates that, defects in DNASE1L3 enhances the accumulation of cytoplasmic DNA and triggers the activation of DNA sensors. However, it maintains the homeostasis through anti-apoptosis.

Evolving eukaryotes developed the ability to maintain homeostasis not just in cells but in the whole organisms too. Homeostatic maintenance leads to a powerful rewiring of adaptive stress responses [34, 35]. Responses to the disturbance of intracellular or extracellular microenvironments, the cells and the body attempt to restore the physiological functions. However, if stress adaptation fails, cells exhibit one of two ultimate destinies: i. cell senescence, corresponding to their irreversible proliferation and inactivation [35, 36]; or ii. regulation of cell death (RCD), through one of a variety of non-exclusive and highly interrelated pathways [35, 37].

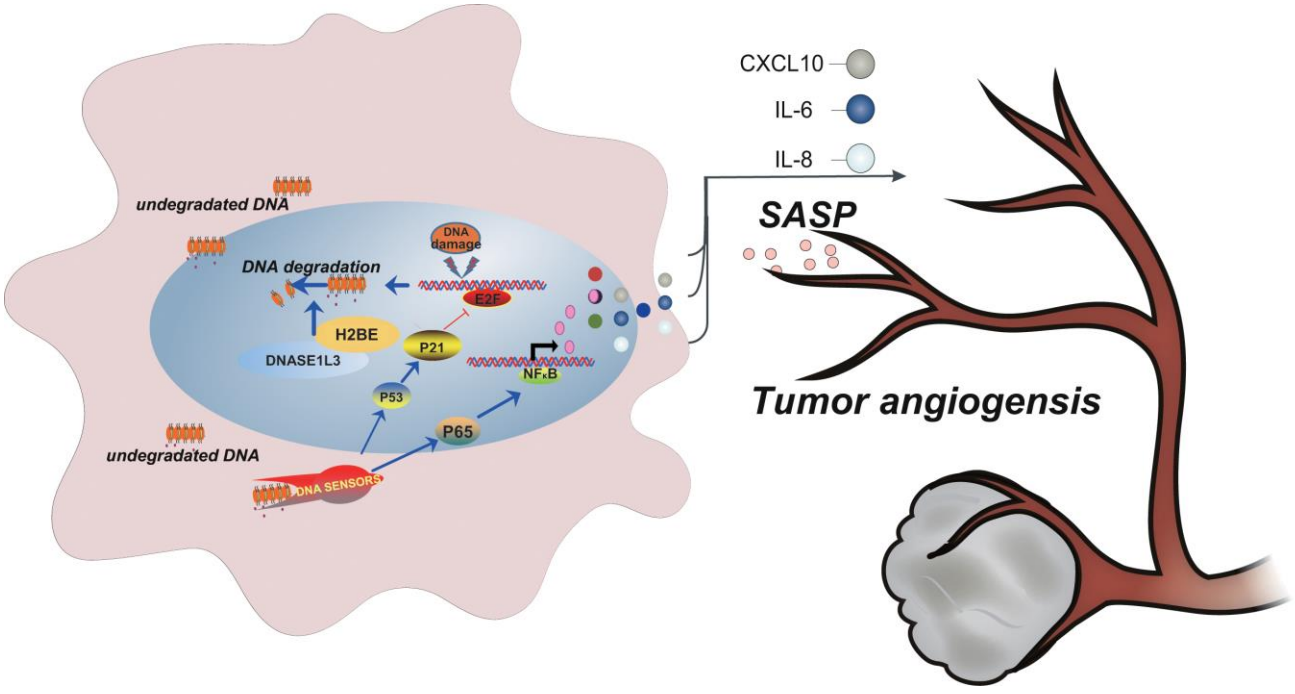

Figure 8. Model depicting DNASE1L3 regulation of tumor angiogenesis by controlling the senescence-associated secretory phenotype in response to stress.

When cellular fitness is irreparably damaged, the dynamic balance between senescence and RCD are used to maintain body homeostasis. However, the outcomes vary and are determined by signal characteristics, spatiotemporal parameters, and cellular capacity to respond [9, 38]. In cases of minor disruptions of cellular processes, brought about by low levels of stress, damage is reversed and the structural and functional integrity of cells restored. Alternatively, damage can be irreversible, causing tissue degeneration and cell death. Between both situations, cells acquire a non-proliferative but viable state, distinct from G0 quiescence and terminal differentiation, with permanent structural and functional changes, termed cellular senescence [9]. But one thing still needs to be pointed out, either the cells undergoing successful (recovery of cellular homeostasis) or unsuccessful (senescence or RCD) responses to stress, they communicate their status to the microenvironment, ultimately affecting organismal adaptation [34].

In our research, cancer cells defected of DNASE1L3 tend to avoid cell death by surpassing apoptotic processes. In contrast, overexpression of DNASE1L3 provokes more cellular apoptosis than senescence during DNA damage. This must be relevant to its function in processing DNA fragmentation from ~50kb into mononucleosome of 153 bp [18]. Low expression of DNASE1L3 decrease the degradation efficiency of unsuccessful repaired DNA to some extent. Thus, in DNASE1L3 relieves the activation of p53-p21 signal pathway and NF-κB pathway via repressing cytoplasmic DNA accumulation during DNA damage. Meanwhile, the DNASE1L3-dependent DNA fragments also provoke the expression of numerous SASP factors and promote tumor angiogenesis. Interestingly, in our retrospective clinical studies of HCC, the reduced DNASE1L3 expression is associated with not only less favorable outcome after hepatectomy, but also the poor prognosis of DNA damage therapy (ischemia and hypoxia, accompanied by oxidative stress and mitochondrial dysfunction induced by TACE [39]) and anti-angiogenic therapy (Sorafenib).

In summary, this study, for the first time, confirms that DNASE1L3 affects the angiogenesis via regulating the expression of numerous SASP factors in response to stress. Mechanistically, during DNA damage, DNASE1L3 translocates to the nucleus, interacts with H2BE, participates in the degradation of unsuccessful repaired DNA, and relieves tumor cell senescence as well as the expression of SASP factors contributed to the microenvironments. Based on these findings, we propose that DNASE1L3 may act as a vital predictive biomarker for associated clinical DNA damage treatments.

MATERIALS AND METHODS

DNA damage treatment and induction of senescence

For ultraviolet (UV) radiation-treatment, approximately 2×10^5 cells was cultured in each well of a 6-well plate. When DNA damage performed, the medium was taken off, cells were irradiated with UVB, 20-30 mJ/cm^2. Then, incubate the cells in 2 mL of DMEM with 10%FBS for another 7 days. For oxidative stress treatment, approximately 2×10^5 cells were cultured and incubated in each well of a 6-well plate. A solution of ~150 μM hydrogen peroxide in complete cell culture was prepared by adding 75 μL of 30% hydrogen peroxide in 50 mL of complete cell culture. When DNA damage performed, the medium of the cells was aspirated and washed once with fresh PBS. Then, 2 mL of DMEM with hydrogen peroxide was added, and incubated for 3 days. The preceding step was repeat twice, and the cells were incubated for another 6 days.

SA-β-Gal staining

SA-β-Gal staining was processed with Senescence β-Galactosidase Staining Kit (Beyotime, China), following the manufacturer's recommendations. Briefly, cells with or without DNA damage treatments were cultured for 7 days. After that, the samples were fixed for 15 min followed by washing the plate or slides with PBS for 3 times. Next, the plates were rinsed with PBS, stained with β-galactosidase staining solution, incubated overnight at 37° C in a dry incubator without CO_2. Then, the slides were rinsed with tap water. Finally, we analyzed the blue staining under a fluorescence microscope.

Fluorescence resonance energy transfer (FRET) assay

HepG2 cells plated on poly-l-lysine–coated glass-bottomed dishes (Beyotime) were cotransfected with reconstructed pEYFP-C1 and pECFP-N1 plasmid. The basic vectors (pEYFP-C1 and pECFP-N1) were used in the control experiments. After cultured for 96 h, they were treated with UV radiation and cultured for another 8 h. Samples were imaged using Leica TCS SP8 confocal microscope equipped with three photomultipliers (PMTs). The laser was tuned to lines 458 and 514 to excite CFP (458 nm) and YFP (514 nm). With a META spectral detector, emission profiles were generated by scanning emission spectra of H2BE-CFP and DNASE1L3-YFP across a series of wavelengths (462 to 633 nm). FRET was measured using acceptor photo-bleaching according to the method reported previously [40]. The FRET efficiency were calculated by Leica TCS SP8 software ($FRET_{eff} = (D_{post}-D_{pre})/D_{pos}$).

Ethics approval and consent to participate

Ethical approval was obtained from Ethics Committee of Zhongnan Hospital of Wuhan University, and written informed consent was obtained from each patient.

Consent for publication

All authors have agreed to publish this manuscript.

Availability of data and materials

The datasets used and analysed during the current study are available from the corresponding author on reasonable request.

Editorial note

[&]This corresponding author has a verified history of publications using a personal email address for correspondence.

Abbreviations

HCC: Hepatocellular carcinoma; DNASE1L3: deoxyribonuclease1-like 3; HBV: hepatitis B virus; HCV: hepatitis C virus; DDR: DNA damage response; NLS: nuclear localization signal; AWERB: Animal Welfare and Ethical Review Body; IHC: immunohistochemistry; UV: ultraviolet; EdU: 5-Ethynyl-2′-deoxyuridine; FRET: Fluorescence resonance energy transfer; TCGA: The Cancer Genome Atlas; qPCR: quantitative real-time PCR; DDF: DNA damage foci; RCD: regulation of cell death.

AUTHOR CONTRIBUTIONS

Quanyan Liu and Zhisu Liu were the principal investigators for the study. Deliang Guo and Dong Ma conceived the study and carried out the major part of the project. Deliang Guo also performed figure editing according to the journal's request. Jianwei Lan participated in this project and collected and analyzed the data. Deliang Guo and Pengpeng Liu wrote the manuscript, collected clinical and experimental data and made significant improvement to the preliminary data. Quanyan Liu and Zhisu Liu provided the funding and contributed to critical review of the manuscript. The authors read and approved the final manuscript.

ACKNOWLEDGMENTS

We acknowledge Ying Zhou (Medical Research Center for Structural Biology of Wuhan University) for assistance in conducting the experiments on the microscopy images.

CONFLICTS OF INTEREST

All the authors declared no conflicts of interest.

FUNDING

This work was supported by grants from the National Natural Science Foundation of China (no. 81872029 and no. 81772926).

REFERENCES

1. Bray F, Ferlay J, Soerjomataram I, Siegel RL, Torre LA, Jemal A. Global cancer statistics 2018: GLOBOCAN estimates of incidence and mortality worldwide for 36 cancers in 185 countries. CA Cancer J Clin. 2018; 68:394–424. https://doi.org/10.3322/caac.21492 PMID:30207593

2. Galle PR, Tovoli F, Foerster F, Wörns MA, Cucchetti A, Bolondi L. The treatment of intermediate stage tumours beyond TACE: from surgery to systemic therapy. J Hepatol. 2017; 67:173–83. https://doi.org/10.1016/j.jhep.2017.03.007 PMID:28323121

3. Reig M, da Fonseca LG, Faivre S. New trials and results in systemic treatment of HCC. J Hepatol. 2018; 69:525–33. https://doi.org/10.1016/j.jhep.2018.03.028 PMID:29653122

4. Lyu N, Kong Y, Mu L, Lin Y, Li J, Liu Y, Zhang Z, Zheng L, Deng H, Li S, Xie Q, Guo R, Shi M, et al. Hepatic arterial infusion of oxaliplatin plus fluorouracil/leucovorin vs. sorafenib for advanced hepatocellular carcinoma. J Hepatol. 2018; 69:60–69. https://doi.org/10.1016/j.jhep.2018.02.008 PMID:29471013

5. Abou-Alfa GK, Qin S, Ryoo BY, Lu SN, Yen CJ, Feng YH, Lim HY, Izzo F, Colombo M, Sarker D, Bolondi L, Vaccaro G, Harris WP, et al. Phase III randomized study of second line ADI-PEG 20 plus best supportive care versus placebo plus best supportive care in patients with advanced hepatocellular carcinoma. Ann Oncol. 2018; 29:1402–08. https://doi.org/10.1093/annonc/mdy101 PMID:29659672

6. Yang JD, Hainaut P, Gores GJ, Amadou A, Plymoth A, Roberts LR. A global view of hepatocellular carcinoma: trends, risk, prevention and management. Nat Rev Gastroenterol Hepatol. 2019; 16:589–604. https://doi.org/10.1038/s41575-019-0186-y

PMID:31439937

7. Gourley C, Balmaña J, Ledermann JA, Serra V, Dent R, Loibl S, Pujade-Lauraine E, Boulton SJ. Moving from poly (ADP-Ribose) polymerase inhibition to targeting DNA repair and DNA damage response in cancer therapy. J Clin Oncol. 2019; 37:2257–69. https://doi.org/10.1200/JCO.18.02050 PMID:31050911

8. Yang SF, Chang CW, Wei RJ, Shiue YL, Wang SN, Yeh YT. Involvement of DNA damage response pathways in hepatocellular carcinoma. Biomed Res Int. 2014; 2014:153867. https://doi.org/10.1155/2014/153867 PMID:24877058

9. Gorgoulis V, Adams PD, Alimonti A, Bennett DC, Bischof O, Bishop C, Campisi J, Collado M, Evangelou K, Ferbeyre G, Gil J, Hara E, Krizhanovsky V, et al. Cellular senescence: Defining a path forward. Cell. 2019; 179:813–27. https://doi.org/10.1016/j.cell.2019.10.005 PMID:31675495

10. Dou Z, Ghosh K, Vizioli MG, Zhu J, Sen P, Wangensteen KJ, Simithy J, Lan Y, Lin Y, Zhou Z, Capell BC, Xu C, Xu M, et al. Cytoplasmic chromatin triggers inflammation in senescence and cancer. Nature. 2017; 550:402–06. https://doi.org/10.1038/nature24050 PMID:28976970

11. Faget DV, Ren Q, Stewart SA. Unmasking senescence: context-dependent effects of SASP in cancer. Nat Rev Cancer. 2019; 19:439–53. https://doi.org/10.1038/s41568-019-0156-2 PMID:31235879

12. Guo M. Cellular senescence and liver disease: Mechanisms and therapeutic strategies. Biomed Pharmacother. 2017; 96:1527–37. https://doi.org/10.1016/j.biopha.2017.11.075 PMID:29174037

13. Zhou BB, Elledge SJ. The DNA damage response: putting checkpoints in perspective. Nature. 2000; 408:433–39. https://doi.org/10.1038/35044005 PMID:11100718

14. Napirei M, Wulf S, Eulitz D, Mannherz HG, Kloeckl T. Comparative characterization of rat deoxyribonuclease 1 (Dnase1) and murine deoxyribonuclease 1-like 3 (Dnase1l3). Biochem J. 2005; 389:355–64. https://doi.org/10.1042/BJ20042124 PMID:15796714

15. Sisirak V, Sally B, D'Agati V, Martinez-Ortiz W, Özçakar ZB, David J, Rashidfarrokhi A, Yeste A, Panea C, Chida AS, Bogunovic M, Ivanov II, Quintana FJ, et al. Digestion of chromatin in apoptotic cell microparticles prevents autoimmunity. Cell. 2016; 166:88–101. https://doi.org/10.1016/j.cell.2016.05.034 PMID:27293190

16. Serpas L, Chan RW, Jiang P, Ni M, Sun K, Rashidfarrokhi A, Soni C, Sisirak V, Lee WS, Cheng SH, Peng W, Chan KC, Chiu RW, et al. *Dnase1l3* deletion causes aberrations in length and end-motif frequencies in plasma DNA. Proc Natl Acad Sci USA. 2019; 116:641–49. https://doi.org/10.1073/pnas.1815031116 PMID:30593563

17. Shiokawa D, Shika Y, Tanuma S. Identification of two functional nuclear localization signals in DNase gamma and their roles in its apoptotic DNase activity. Biochem J. 2003; 376:377–81. https://doi.org/10.1042/BJ20030820 PMID:12943533

18. Chan RW, Serpas L, Ni M, Volpi S, Hiraki LT, Tam LS, Rashidfarrokhi A, Wong PC, Tam LH, Wang Y, Jiang P, Cheng AS, Peng W, et al. Plasma DNA profile associated with DNASE1L3 gene mutations: clinical observations, relationships to nuclease substrate preference, and *in vivo* correction. Am J Hum Genet. 2020; 107:882–94. https://doi.org/10.1016/j.ajhg.2020.09.006 PMID:33022220

19. Menyhárt O, Nagy Á, Győrffy B. Determining consistent prognostic biomarkers of overall survival and vascular invasion in hepatocellular carcinoma. R Soc Open Sci. 2018; 5:181006. https://doi.org/10.1098/rsos.181006 PMID:30662724

20. Takahashi A, Loo TM, Okada R, Kamachi F, Watanabe Y, Wakita M, Watanabe S, Kawamoto S, Miyata K, Barber GN, Ohtani N, Hara E. Downregulation of cytoplasmic DNases is implicated in cytoplasmic DNA accumulation and SASP in senescent cells. Nat Commun. 2018; 9:1249. https://doi.org/10.1038/s41467-018-03555-8 PMID:29593264

21. Childs BG, Baker DJ, Kirkland JL, Campisi J, van Deursen JM. Senescence and apoptosis: dueling or complementary cell fates? EMBO Rep. 2014; 15:1139–53. https://doi.org/10.15252/embr.201439245 PMID:25312810

22. Takahashi A, Okada R, Nagao K, Kawamata Y, Hanyu A, Yoshimoto S, Takasugi M, Watanabe S, Kanemaki MT, Obuse C, Hara E. Exosomes maintain cellular homeostasis by excreting harmful DNA from cells. Nat Commun. 2017; 8:15287. https://doi.org/10.1038/ncomms15287 PMID:28508895

23. Zhang B, Fu D, Xu Q, Cong X, Wu C, Zhong X, Ma Y, Lv Z, Chen F, Han L, Qian M, Chin YE, Lam EW, et al. The senescence-associated secretory phenotype is potentiated by feedforward regulatory mechanisms involving Zscan4 and TAK1. Nat Commun. 2018; 9:1723.

https://doi.org/10.1038/s41467-018-04010-4
PMID:29712904

24. Malecki M, Dahlke J, Haig M, Wohlwend L, Malecki R. Eradication of Human Ovarian Cancer Cells by Transgenic Expression of Recombinant DNASE1, DNASE1L3, DNASE2, and DFFB Controlled by EGFR Promoter: Novel Strategy for Targeted Therapy of Cancer. J Genet Syndr Gene Ther. 2013; 4:152. https://doi.org/10.4172/2157-7412.1000152 PMID:24587967

25. Boulares H, Zoltoski A, Kandan S, Akbulut T, Yakovlev A, Oumouna M. Correlation between decreased sensitivity of the Daudi lymphoma cells to VP-16-induced apoptosis and deficiency in DNAS1L3 expression. Biochem Biophys Res Commun. 2006; 341:653–62. https://doi.org/10.1016/j.bbrc.2006.01.014 PMID:16427601

26. Fasci D, van Ingen H, Scheltema RA, Heck AJ. Histone interaction landscapes visualized by crosslinking mass spectrometry in intact cell nuclei. Mol Cell Proteomics. 2018; 17:2018–33. https://doi.org/10.1074/mcp.RA118.000924 PMID:30021884

27. Shi G, Abbott KN, Wu W, Salter RD, Keyel PA. Dnase1L3 regulates inflammasome-dependent cytokine secretion. Front Immunol. 2017; 8:522. https://doi.org/10.3389/fimmu.2017.00522 PMID:28533778

28. Errami Y, Naura AS, Kim H, Ju J, Suzuki Y, El-Bahrawy AH, Ghonim MA, Hemeida RA, Mansy MS, Zhang J, Xu M, Smulson ME, Brim H, Boulares AH. Apoptotic DNA fragmentation may be a cooperative activity between caspase-activated deoxyribonuclease and the poly(ADP-ribose) polymerase-regulated DNAS1L3, an endoplasmic reticulum-localized endonuclease that translocates to the nucleus during apoptosis. J Biol Chem. 2013; 288:3460–8. https://doi.org/10.1074/jbc.M112.423061 PMID:23229555

29. Han DS, Ni M, Chan RW, Chan VW, Lui KO, Chiu RW, Lo YM. The biology of cell-free DNA fragmentation and the roles of DNASE1, DNASE1L3, and DFFB. Am J Hum Genet. 2020; 106:202–14. https://doi.org/10.1016/j.ajhg.2020.01.008 PMID:32004449

30. Widłak P. The DFF40/CAD endonuclease and its role in apoptosis. Acta Biochim Pol. 2000; 47:1037–44. PMID:11996094

31. Nagata S, Kawane K. Autoinflammation by endogenous DNA. Adv Immunol. 2011; 110:139–61. https://doi.org/10.1016/B978-0-12-387663-8.00004-1 PMID:21762818

32. Boulares AH, Ren T. Mechanism of acetaminophen-induced apoptosis in cultured cells: roles of caspase-3, DNA fragmentation factor, and the Ca2+ and Mg2+ endonuclease DNAS1L3. Basic Clin Pharmacol Toxicol. 2004; 94:19–29. PMID:14725611

33. Watanabe T, Takada S, Mizuta R. Cell-free DNA in blood circulation is generated by DNase1L3 and caspase-activated DNase. Biochem Biophys Res Commun. 2019; 516:790–95. https://doi.org/10.1016/j.bbrc.2019.06.069 PMID:31255286

34. Galluzzi L, Yamazaki T, Kroemer G. Linking cellular stress responses to systemic homeostasis. Nat Rev Mol Cell Biol. 2018; 19:731–45. https://doi.org/10.1038/s41580-018-0068-0 PMID:30305710

35. Vanpouille-Box C, Demaria S, Formenti SC, Galluzzi L. Cytosolic DNA sensing in organismal tumor control. Cancer Cell. 2018; 34:361–78. https://doi.org/10.1016/j.ccell.2018.05.013 PMID:30216189

36. Muñoz-Espín D, Serrano M. Cellular senescence: from physiology to pathology. Nat Rev Mol Cell Biol. 2014; 15:482–96. https://doi.org/10.1038/nrm3823 PMID:24954210

37. Fuchs Y, Steller H. Live to die another way: modes of programmed cell death and the signals emanating from dying cells. Nat Rev Mol Cell Biol. 2015; 16:329–44. https://doi.org/10.1038/nrm3999 PMID:25991373

38. Gorgoulis VG, Pefani DE, Pateras IS, Trougakos IP. Integrating the DNA damage and protein stress responses during cancer development and treatment. J Pathol. 2018; 246:12–40. https://doi.org/10.1002/path.5097 PMID:29756349

39. Xiao L, Wang M. Batimastat nanoparticles associated with transcatheter arterial chemoembolization decrease hepatocellular carcinoma recurrence. Cell Biochem Biophys. 2014; 70:269–72. https://doi.org/10.1007/s12013-014-9893-8 PMID:24639109

40. Karpova TS, Baumann CT, He L, Wu X, Grammer A, Lipsky P, Hager GL, McNally JG. Fluorescence resonance energy transfer from cyan to yellow fluorescent protein detected by acceptor photobleaching using confocal microscopy and a single

laser. J Microsc. 2003; 209:56–70.
https://doi.org/10.1046/j.1365-2818.2003.01100.x
PMID:12535185

SUPPLEMENTARY MATERIALS

Supplementary Methods

Ethical application

Use of human subjects

Written informed consent was given by all participating patients or their legal representatives. Ethics committee approval was obtained from the ethics committee of Zhongnan Hospital.

Use of experimental animals

All animal experiments were approved by the Wuhan University Animal Welfare and Ethical Review Body (AWERB) and the study was approved by the home office. All animal care and experimental procedures were in accordance with Roche guidelines and national/international guidelines for animal care.

Cell lines and culture

The human hepatocellular carcinoma cell line HepG2, SMMC7721, SNU-387, HepG2.2.15, HCCLM3, HCCLM9, Huh7 and mouse hepatocellular carcinoma cell line Hepa1-6 as well as HEK293T and THLE-3 were all grown in DMEM (HyClone, USA) supplemented with 10% fetal bovine serum(FBS) (HyClone, USA). Cells were cultured in monolayers in 75 cm^2 or 10 cm culture dishes humidified atmosphere containing 5% CO_2.

Cell culture supernatant concentration and extraction

The supernatants of cells in different groups treated with or without UV or H2O2 after 7days were collected and centrifuged at 1,000 g × 10 minutes. After that, the centrifuged supernatant was filtered by Amicon Ultra filter device (Millipore, USA), centrifuged at 4,500 g × 30 minutes. To this point, concentrated protein-containing liquid was obtained.

Immunofluorescence and immunohistochemistry (IHC)

HCC specimens were obtained from 204 patients (aged from 18-80 y) accepted curative liver resection operation in Zhongnan Hospital of Wuhan University in Wuhan, China. No patients underwent preoperative anti-cancer treatment. For Immunofluorescence analysis, cells grown on coverslips were treated according to previous method [1]. For immunohistochemical analysis, formalin-fixed paraffin embedded tissue microarray slides from HCC patients were probed with DNASE1L3 antibody (ab203669, Abcam). Formalin-fixed paraffin-embedded samples were also obtained from xenograft tumors and then probed with antibodies against CD34 (ab81289, Abcam). After that, positive cells were identified with DAB+ as a chromogen. To analyze the expression level of DNASE1L3 and CD34, slides were scanned by Aperio ScanScope (Aperio) scored modifying a method as previously reported [1].

Plasmid constructions

Full-length sequence of DNASE1L3 with a C-terminal Myc tag and H2BE with a N-terminal Flag tag was cloned into pcDNA3.1(-) separately. Deletion mutants of H2BE, H2BEΔ29-126 with a N-terminal Flag tag were constructed by PCR and cloned into pcDNA3.1(-). For the FRET assay, the full-length sequence of DNASE1L3 and H2BE were cloned into pEYFP-C1 and pECFP-N1 separately. For shRNA experiments, oligonucleotides targeting homo sapiens DNASE1L3(1# 5′- GGCTTGG AAGAAACACATA -3′; 2# 5′- GCATAACGTACAA CTATGT -3′), were annealed and cloned into the pENTR/U6 shRNA vector.

Quantitative real-time PCR

Total RNA was extracted from cultured cells and tissues by TRIzol reagent (Invitrogen) and reverse transcribed into cDNA by HiScript® III 1st Strand cDNA Synthesis Kit (+gDNA wiper) (Vazyme). RT-PCR was performed using ChamQTMSYBR®qPCR Master Mix (High ROX Premixed) (Vazyme). All PCR primers are summarized in Supplementary Table 3.

Isolation of cytosol DNA fractions

Cytoplasmic DNA was extracted according to a previously reported method [2]. Briefly, cells were centrifuged at 200g × 5 min, suspended and homogenized in 0.3 M sucrose buffer, overlaid on 1.5 M sucrose buffer, centrifuged at 18,506 g ×10 min, purified by 0.4 mg/ml Proteinase K (Beyotime) treatment, phenol/chloroform extraction and ethanol precipitation with a carrier (Dr. GenTLE® Precipitation Carrier, Takara Bio Inc.). RT-qPCR was used to assess the amount of cytoplasmic DNA [2]. The PCR primers for human chromosome 3, 10, and 13 are shown in Supplementary Table 3.

Western blot analysis

Cells or tumor tissues were lysed in RIPA lysis buffer with 1% Protease inhibitor cocktail (Beyotime, China). The protein concentration was obtained by bicinchoninic acid (BCA) assay (Beyotime, China). Then the samples were separated by SDS-PAGE and transferred onto a PVDF membrane (Millipore, USA). Membranes were

probed with appropriate dilutions of specific primary antibodies overnight at 4° C, then HRP-conjugated secondary antibodies were used for further detection. The primary antibodies used in this assay are listed in Supplementary Table 4.

ELISA assay

Cells were counted for normalization followed by cell culture supernatant collected as previously illustrated. Human IL-6, IL-8 immunoassay was tested using kits per the manufacturer's instructions. (Proteintech, China).

Coimmunoprecipitation

To evaluate the interaction between DNASE1L3 and H2BE, plasmids Flag-H2BE and cMyc-DNASE1L3 were cotransfected into HEK 293T cells. Lysates of HepG2, HCCLM3, HEK293T cells were pre-cleaned and then coimmunoprecipitation was performed with the Pierce Co-Immunoprecipitation kit (Thermo Scientific). The lysates in IP lysis buffer were incubated with anti-Flag, anti-Myc, anti-H2BE antibodies or IgG overnight at 4° C, then the proteins were eluted in 60 μl and separated by western blotting.

NF-κB reporter assays

NF-κB transcription activity was identified by luciferase signals derived from a pNF-kB-TA-Luc construct that encodes multiple copies of NF-κB binding sequences. pGL4.70(hRluc) plasmid was co-transfected for transfection efficiency controls. Luciferase activities of cell lysates were tested using a luminometer and Dual Luciferase Reporter Gene Assay Kit (Beyotime), according to the manufacturer's instructions.

Flow cytometric analysis

HepG2 and HCCLM9 cells transfected with vector or DNASE1L3 were treated with or without H2O2 or UV treatments. After that, cells were continued cultured for another 24 hours and harvested. Samples were stained with an annexin V-FITC/PI apoptosis kit (MultiSciences). The cells were then analyzed by flow cytometry to identify apoptosis (Beckman Coulter).

5-Ethynyl-2′-deoxyuridine (EdU) incorporation assay

EdU incorporation assay was operated using the BeyoClick™ EdU-594 imaging detection kit (Beyotime, China). HepG2 and HCCLM9 cells transfected with vector or DNASE1L3 treated with H2O2 or UV treatments were cultured for another 24 hours after DNA damage treatments, then EdU labelling medium was added and incubated for 24 hours. The cells were proceeding as the manufacturer's instructions recommended.

Wound healing assay

HUVECs were suspended in DMEM with 10% FBS, and seeded at a density of 500,000 cells per well in 6-well culture plates. Upon reaching 100% confluence, wounds were made using a 200 μl plastic pipette tip. The medium was then changed to DMEM mixed with concentrated supernatant from different groups and incubated for further tests. Photos were recorded at 0 and 24 h.

Cell migration assay

Cell migration assays were performed using transwell chambers (8-μm pore size; Corning) in 24 well plates. In the lower chamber, concentrated cell culture supernatants from different groups were mixed in complete culture separately; in the upper chamber, approximately 50,000 HUVECs suspended in DMEM were added. After incubated for another 24 hours, the cells in the upper chamber were fixed with methanol and stained with 0.1% crystal violet. Cells on the upper side of the transwell membrane were wiped off with a cotton swab, cells on the underside of the transwell membrane were photographed and quantified under a microscope.

Tube formation assay

200 μl of Matrigel (Corning® Matrigel® Matrix, USA) was added to each well of a 24-well plate. HUVECs were suspended in DMEM mixed with concentrated cell culture supernatant from different groups and seeded onto the Matrigel at the density of 200,000 cells per well followed by the Matrigel polymerized in the incubator for 60 min. Then, the cells were incubated for 6 h, tubes were visualized under a microscope and the meshes formed by HUVECs were quantified.

Subcellular fractionation assay

The separation of nucleus-cytoplasm in HepG2 and HCCLM3 cells were performed following the manufacturer's instructions of the PARIS Kit (Invitrogen). β-Tublin and H3 were employed as the indicators for quantification of the fractions.

Matrigel plug assay

To evaluate the angiogenic response *in vivo*, matrigel growth factor reduced (0.40 mL, Corning) mixed with heparin (10 U/mL), a total of 10^6 HUVECs and concentrated cell culture supernatant (0.1mL) from

different groups were mixed separately and subcutaneously injected into the flanks of 6-week-old BALB/c nude mice (Vital River, Beijing, China). On day 10 post injection, matrigel plugs were removed and sliced into two parts, hemoglobin quantities were then evaluated. The other parts of matrigel plugs were fixed in formalin and embedded with paraffin for the followed IHC assays.

In vivo assay

For tumor angiogenesis assay *in vivo*, Hepa1-6 cells were subcutaneously injected into 5-week-old male BALB/c nude mice (Vital River, Beijing, China) to induce tumor formations. The model was established after feeding for a week. Then, concentrated cell culture supernatants from different groups were separately injected via tail vein for the subsequent two weeks (twice per week, for 2 weeks for a total of four doses). Mice were sacrificed at 8 weeks. The vascular density was quantified by CD34 Chalkley count under IHC.

Bioinformatics data analysis

For TCGA analyses, RNA sequencing datasets were obtained from cBioportal (www.cbioportal.org). The expression data of DNASE1L3 were log2TPM transformed and compared between tumors and normal tissues. The OS and RFS time results were obtained from GEPIA web server [3]. For the cohort of HCC patients treated with sorafenib, a total of 364 cases were enrolled and 30 patients who had been subjected to sorafenib treatment were selected. Liver cancer RNA-seq data, OS time and PFS time were analyzed using KM plotter [4].

Statistical analysis

Data were shown as means±SD or as a percentage from at least three independent experiments. IBM SPSS statistical software (IBM Corporation, USA) and GraphPad Prism (GraphPad Software, USA) were used to perform the statistical analysis. The relationship between DNASE1L3 expression and clinicopathological characteristics was determined using chi-Square test. Differences between experimental groups were assessed by Student's t-test or one-way ANOVA. Survival time was calculated by Kaplan-Meier and log-rank tests. Independent predictors of OS time were detected using Cox regression analysis (the criteria for the entry into the logistic regression model was $P < 0.05$). Statistical significance was set at $^{*}P < 0.05$, $^{**}P < 0.01$, $^{***}P < 0.001$.

Supplementary References

1. Ma Z, Guo D, Wang Q, Liu P, Xiao Y, Wu P, Wang Y, Chen B, Liu Z, Liu Q. Lgr5-mediated p53 repression through PDCD5 leads to doxorubicin resistance in hepatocellular carcinoma. Theranostics. 2019; 9:2967–83. https://doi.org/10.7150/thno.30562 PMID:31244936

2. Takahashi A, Loo TM, Okada R, Kamachi F, Watanabe Y, Wakita M, Watanabe S, Kawamoto S, Miyata K, Barber GN, Ohtani N, Hara E. Downregulation of cytoplasmic DNases is implicated in cytoplasmic DNA accumulation and SASP in senescent cells. Nat Commun. 2018; 9:1249. https://doi.org/10.1038/s41467-018-03555-8 PMID:29593264

3. Tang Z, Li C, Kang B, Gao G, Li C, Zhang Z. GEPIA: a web server for cancer and normal gene expression profiling and interactive analyses. Nucleic Acids Res. 2017; 45:W98–102. https://doi.org/10.1093/nar/gkx247 PMID:28407145

4. Menyhárt O, Nagy Á, Győrffy B. Determining consistent prognostic biomarkers of overall survival and vascular invasion in hepatocellular carcinoma. R Soc Open Sci. 2018; 5. https://doi.org/10.1098/rsos.181006 PMID:30662724

Supplementary Figures

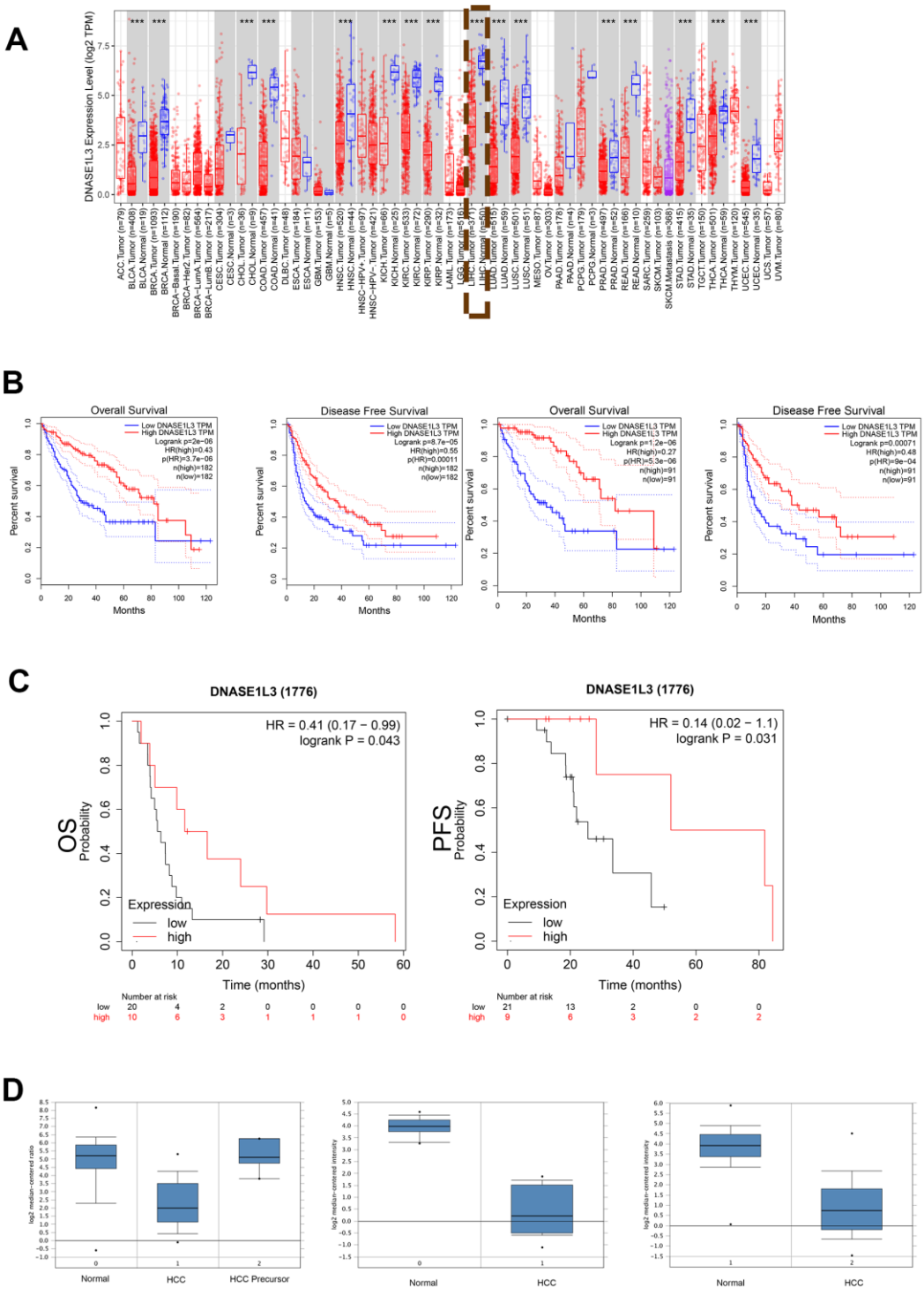

Supplementary Figure 1. (**A**) The mRNA of DNASE1L3 is low expressed in multiple types of tumors from TCGA database. The green dotted frame showed the expression of DNASE1L3 in Liver hepatocellular carcinoma (LIHC). (**B**) Kaplan-Meier curves for overall survival and disease-free survival in HCC patients from the TCGA database showed patients with higher mRNA expression of DNASE1L3 had a better prognosis than those with lower expression. (**C**) OS and PFS in cohort of patients treated with sorafenib, the results indicate low expression of DNASE1L3 is associated with lower insensitivity of sorafenib treatment. (**D**) The mRNA of DNASE1L3 is low expressed in multiple cohorts from Oncomine database. Left, Chen's cohort; Middle, Roessler's cohort1; Right, Roessler's cohort2.

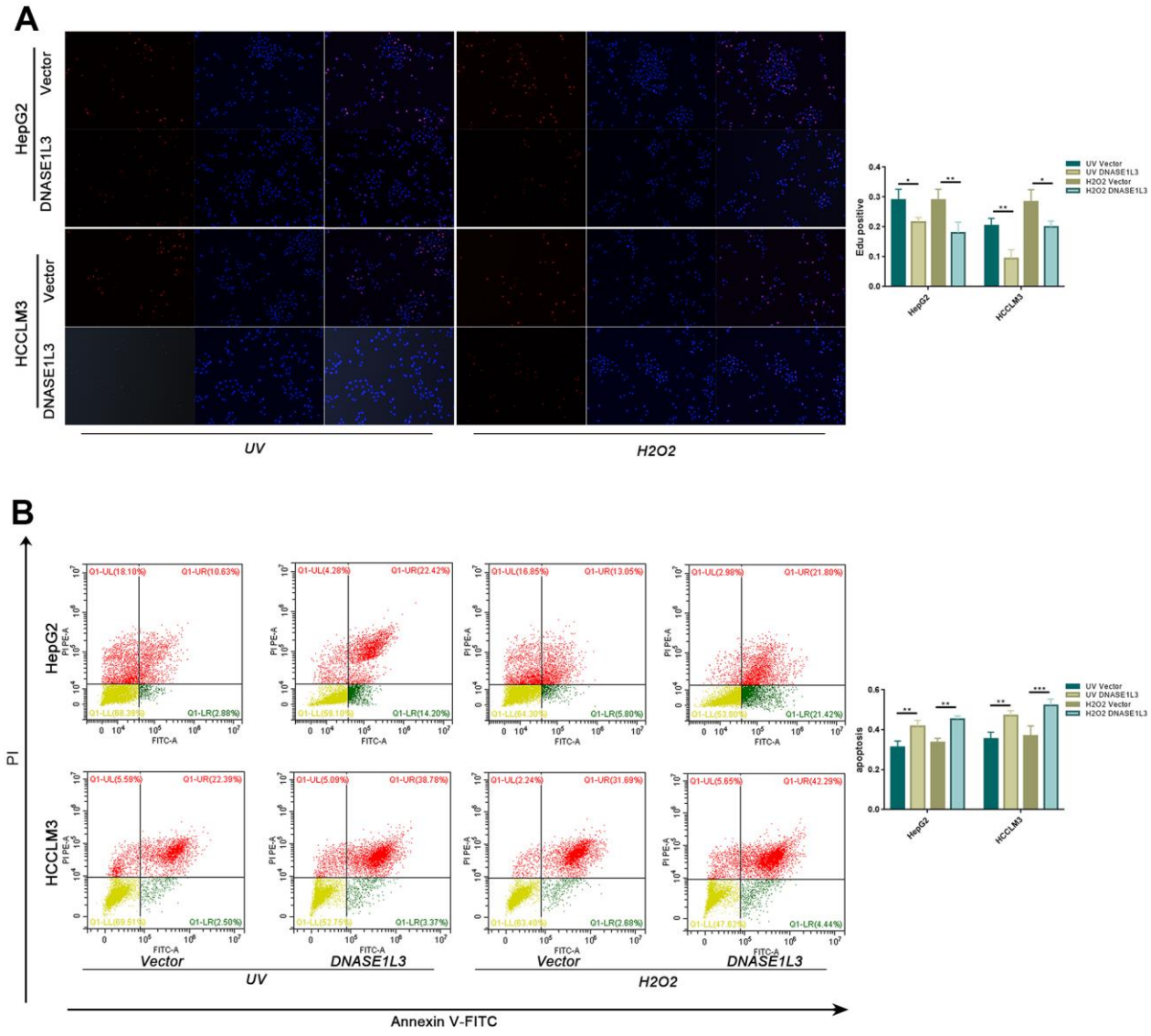

Supplementary Figure 2. (**A**) Reduced DNA synthesis in cells treated in different groups were assessed, representative images were shown (red, Edu; blue, DAPI; 10×). (**B**) Overexpression of DNASE1L3 promotes the apoptosis of cells post DNA damage in the early stage (data were obtained on day2 after DNA damage treatments).

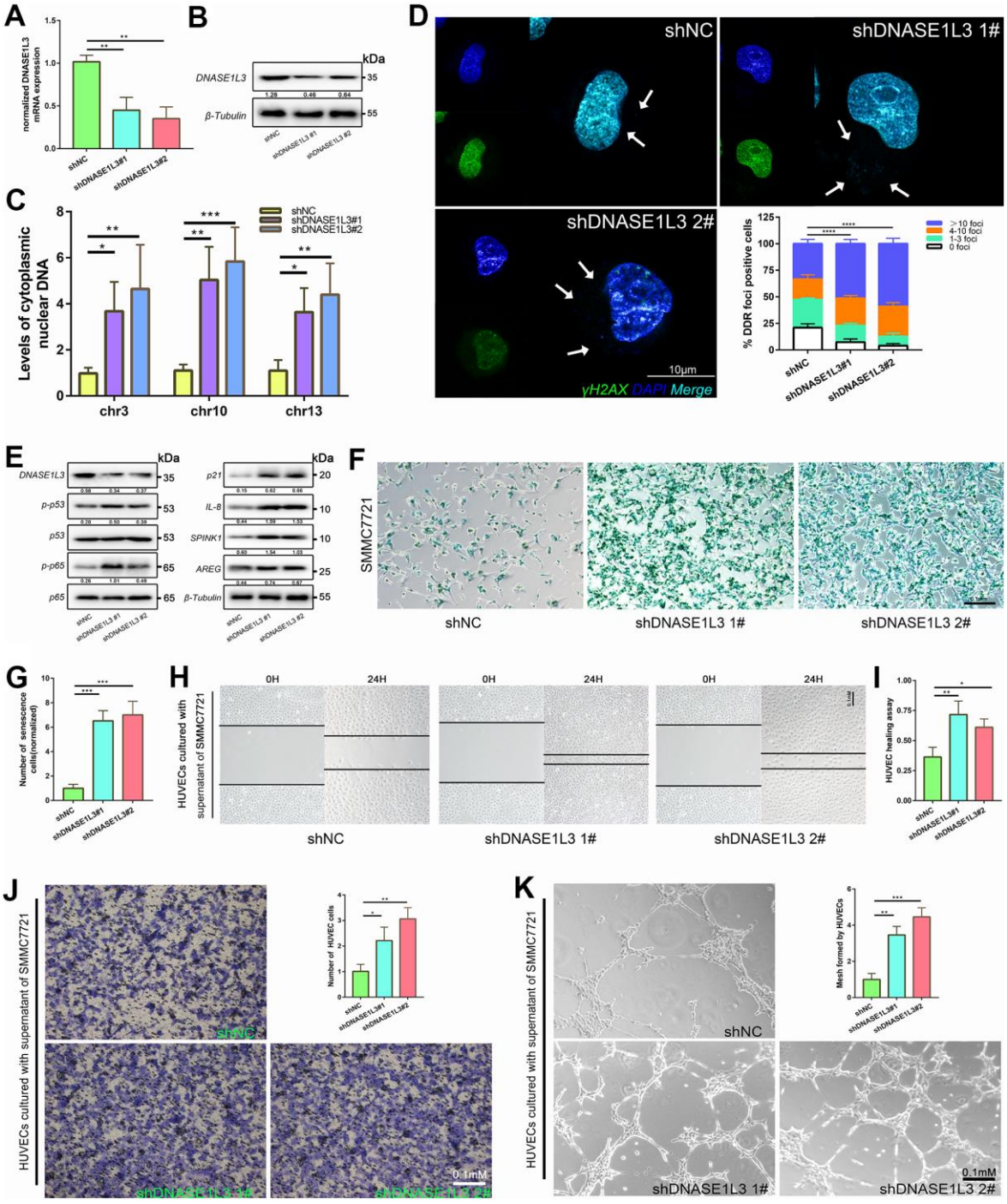

Supplementary Figure 3. (**A**, **B**) DNASE1L3 knockdown in SMMC7721 cell using shRNA(sh)-mediated interference. (**C**) qPCR analysis of chromosomal DNA in cytoplasmic fraction of cells treated in different group. (**D**) Cytoplasmic accumulation of nuclear DNA in differentially treated cells were assessed, representative images were shown (green, γH2AX; blue, DAPI; Scale bars, 10 μm). The number of DNA damage foci (DDF) per cell falls into each of the 0, 1-3, 4-10, and >10 counting categories when quantified the DDF. (**E**) Immunoblot analysis of inducible expression change of senescence associated signal pathway and downstream proteins including p53, p65, SPINK1 and AREG in different treated groups. (**F**) SA-β-Gal staining of cells in differently treated groups (scale bar, 200 μm). (**G**) Statistics of SA-β-Gal staining cells in differently treated groups. (**H**, **I**) The motility of HUVECs were assessed by wound healing assay, the supernatants from cells in differently treated groups were added into the culture of HUVECs, images were taken at 0h and 24h (scale bar, 100 μm). (**J**) The cellular migration ability of HUVECs were determined by the transwell migration assay. The supernatants from cells in differently treated groups were added into the lower chamber, images were taken after 24h of incubation (scale bar, 100 μm). (**K**) The tube formation ability of HUVECs were determined by tube formation assay. The supernatants from cells in differently treated groups were added into the culture, images were taken after 6h of incubation (scale bar, 100 μm). The results show the means ± SD from at least three separate experiments.

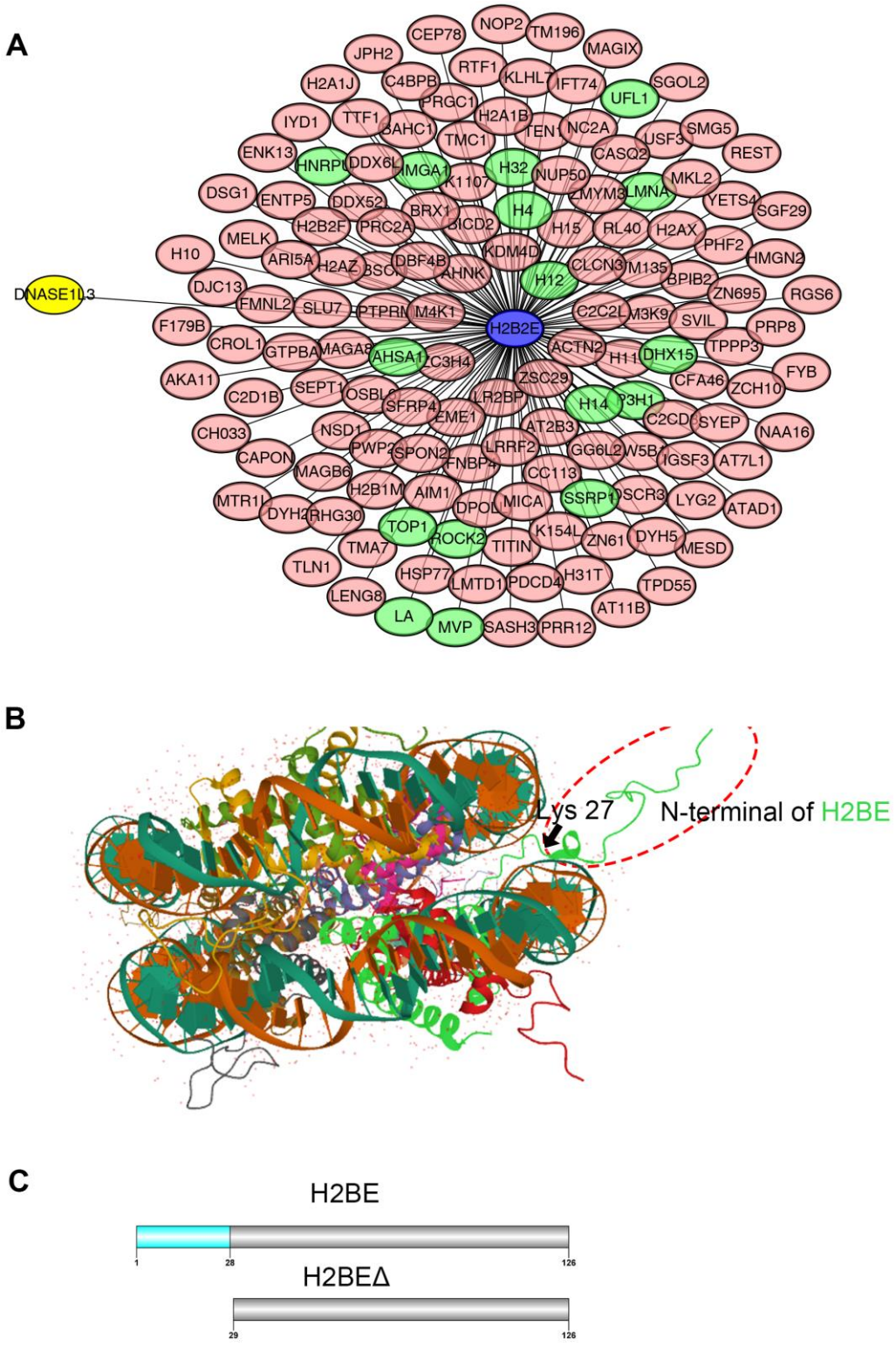

Supplementary Figure 4. (**A**) IntAct Molecular Interaction Database were analyzed (https://www.ebi.ac.uk/intact/interaction/EBI-20919708) and a PPI network was constructed. For the PPI network, network nodes represent proteins, and edges represent protein-protein associations. The DSSO crosslink assay show DNASE1L3 could binding to H2BE, and H2BE binding to other proteins. The nodes colored in green means the protein was also captured in our coIP-MS assay from another unpublished work. (**B**) The N-terminal region of H2BE (amino acids 1-28) is the area on the protein surface, and it is not winded by DNA sequence. The red dotted frame showed the N-terminal region of H2BE in the 3D model. The 3D model of H2BE is downloaded from RCSB database (https://www.rcsb.org/3d-view/1KX5). (**C**) Reconstructed H2BEΔ with the N-terminal region deleted.

Supplementary Tables

Supplementary Table 1. Tumor parameters of the DNASE1L3 high-expression and low-expression groups.

Parameters	DNASE1L3 expression		Total	*P* value
	High(n=102)	Low(n=102)		
Age(y)				0.376
≤55	64	70	134	
>55	38	32	70	
Gender				0.452
Male	83	87	170	
Female	19	15	34	
HBV DNA load, (IU/ml)				**0.007***
≤10^4	54	35	89	
>10^4	48	67	115	
AFP (ng/mL)				0.092
≤400	60	48	108	
>400	42	54	96	
Liver cirrhosis				**0.672**
yes	56	59	115	
no	46	43	89	
Tumor size(cm)				**<0.001***
≤5	65	23	88	
>5	37	79	116	
No. of tumors				**0.038***
Solitary	87	75	162	
Multiple	15	27	42	
MVI				**<0.001***
Presence	14	46	60	
Absence	88	56	144	
Edmondson-Steiner classification				**<0.001***
I-II	62	32	94	
III-IV	40	70	110	

* Significant results ($P < 0.05$) are given in bold.

Abbreviation: HBV, hepatitis B virus; MVI, microvascular invasion.

Supplementary Table 2. Univariate and multivariate analysis with a Cox proportional hazard regression model for overall survival.

variable	Univariate analysis			Multivariate analysis		
	HR	95%CI	*P* value	HR	95%CI	*P* value
Age	0.821	0.564-1.195	0.303	-	-	-
Gender	0.856	0.545-1.345	0.500	-	-	-
HBV DNA load	1.105	0.778-1.570	0.577	-	-	-
AFP	1.376	0.972-1.948	0.072	-	-	-
Liver cirrhosis	0.827	0.583-1.172	0.285	-	-	-
Tumor size	1.712	1.194-2.453	**0.003***	1.047	0.698-1.570	0.826
No. of tumors	2.122	1.406-3.202	**<0.001***	2.064	1.355-3.145	**0.001***
MVI	2.028	1.407-2.923	**<0.001***	1.636	1.101-2.430	**0.015***
Edmondson-Steiner classification	1.657	1.161-2.366	**0.005***	1.458	1.004-2.119	**0.048***
DNASE1L3 expression	0.378	0.264-0.540	**<0.001***	0.519	0.337-0.801	**0.003***

* Significant results (P < 0.05) are given in bold.
Abbreviations: HR, hazard risk ratio; CI, confidence interval.

Supplementary Table 3. List of the primers used in this study.

Target gene		Primer (5'-3')
GAPDH	F	GTCTCCTCTGACTTCAACAGCG
	R	ACCACCCTGTTGCTGTAGCCAA
DNASE1L3	F	TGGTTGAGGTCTACACGGACGT
	R	GTCAGTCCTCAAGCGGATGTTC
p16	F	CTCGTGCTGATGCTACTGAGGA
	R	GGTCGGCGCAGTTGGGCTCC
p21	F	AGGTGGACCTGGAGACTCTCAG
	R	TCCTCTTGGAGAAGATCAGCCG
IFN-β	F	CTTGGATTCCTACAAAGAAGCAGC
	R	TCCTCCTTCTGGAACTGCTGCA
CXCL10	F	GGTGAGAAGAGATGTCTGAATCC
	R	GTCCATCCTTGGAAGCACTGCA
IL-1β	F	CCACAGACCTTCCAGGAGAATG
	R	GTGCAGTTCAGTGATCGTACAGG
IL-6	F	AGACAGCCACTCACCTCTTCAG
	R	TTCTGCCAGTGCCTCTTTGCTG
IL-8	F	GAGAGTGATTGAGAGTGGACCAC
	R	CACAACCCTCTGCACCCAGTTT
Chr-3	F	TCAAGTGCCACATCCTATGC
	R	ATTTTTCTAGCCAGGCACCA
Chr-10	F	ACCTGGAAATGGCTGAAATG
	R	AAGTCCTCGCAGAGGTTTCA
Chr-13	F	CGCCAGTGTGTGTAGCACTT
	R	TCGGCCTCTCTCAGTTCTGT

Supplementary Table 4. List of the antibodies used in this study.

Antibody	Source	Dilutions
DNASE1L3	Abcam(ab203669)	IHC:1/100
DNASE1L3	Proteintech(67041-1-Ig)	WB: 1/500
Beta-Tublin	Proteintech(10094-1-AP)	WB: 1/1000
p-p53	Proteintech(28961-1-AP)	WB: 1/1000
p53	Proteintech(60283-2-Ig)	WB: 1/2000
p-p65	Abcam (ab76302)	WB: 1/1000
p65	Proteintech(66535-1-Ig)	WB: 1/1000
p21	Proteintech(60214-1-Ig)	WB: 1/500
IL-8	Abcam (ab110727)	WB: 1/1000
SPINK1	Abcam (ab207302)	WB: 1/5000
AREG	Abcam (ab213698)	WB: 1/1000
anti-Flag	Proteintech(20543-1-AP)	WB: 1/200
anti-C-Myc	Abcam (ab32072)	WB: 1/1000
H2BE	Abcam (ab1790)	WB: 1/1000
H3	Abclonal(A2348)	WB: 1/500